Title
Glycolytic Metabolism Plays a Functional Role in Regulating Human Pluripotent Stem Cell State

Author
Gu, Wen

Publication Date
2017

Peer reviewed|Thesis/dissertation

UNIVERSITY OF CALIFORNIA

Los Angeles

Glycolytic Metabolism Plays a Functional Role in Regulating Human Pluripotent Stem Cell State

A dissertation submitted in partial satisfaction of the

requirements for the degree Doctor of Philosophy

in Molecular and Medical Pharmacology

by

Wen Gu

2017

ABSTRACT OF THE DISSERTATION

Glycolytic Metabolism Plays a Functional Role in Regulating Human Pluripotent Stem Cell State

by

Wen Gu

Doctor of Philosophy in Molecular and Medical Pharmacology

University of California, Los Angeles, 2017

Professor Heather R. Christofk, Chair

The rate of glycolytic metabolism changes during differentiation of human embryonic stem cells (hESCs) and reprogramming of somatic cells to pluripotent stem cells. However, the functional contribution of glycolytic metabolism to pluripotency is unclear. Here we show that the degree of pluripotency is associated with glycolytic rate, whereby naive hESCs exhibit increased glycolytic flux, MYC transcriptional activity, and nuclear localization of N-MYC relative to primed hESCs. This is consistent with the inner cell mass of human blastocysts which exhibit increased MYC transcriptional activity relative primed hESCs and elevated nuclear N-MYC levels. Reduction of glycolysis decreases self-renewal of naive hESCs and feeder-free cultured primed hESCs, but not primed hESCs grown in feeder-supported conditions. Reduction of glycolysis in feeder-free primed hESCs also enhances neural specification. These findings reveal associations between glycolytic metabolism and the state of pluripotency, differences in

the metabolism of feeder- versus feeder-free cultured hESCs, and identify methods for regulating self-renewal and initial cell fate specification of hESCs.

The dissertation of Wen Gu is approved.

Steven J. Bensinger

Amander T. Clark

Thomas G. Graeber

Michael A. Teitell

Heather R. Christofk, Committee Chair

University of California, Los Angeles

2017

DEDICATION

To Huaying, who embodies intellectual curiosity

TABLE OF CONTENTS

LIST OF FIGURES

ACKNOWLEDGEMENTS

I would like to thank my mentor Dr. Heather Christofk, for supporting my graduate studies in the past six years, during which I encountered many roadblocks and setbacks. At every turn, she provided much needed intellectual guidance and financial support for my research project. Many of her brilliant ideas propelled this study forward at times when it seemed stuck. More importantly, she did the best she could to help me succeed in graduate school and beyond. She took the time to teach me how to write grant applications, deliver a good oral presentation, and write research papers and address reviews. She also avidly introduced my work to other experts in the field, and helped me prepare for postdoctoral interviews. I feel extremely fortunate to have her as my mentor, whom I know I could always go to for science and career advice even after graduate school.

I appreciate the comments and suggestions of my thesis committee members: Drs. Steve Bensinger, Amander Clark, Tom Graeber, and Mike Teitell. I am especially grateful to Steve for allowing me to use the resources in his lab; to Amander for getting me started on stem cell research, teaching me proposal writing from her own experience, and helping me get access to precious human blastocyst samples; to Tom for teaching me data analysis skills; and to Mike for strategizing with Heather and I for my project at its early stage.

Although not a mentor on my thesis committee, Dr. Bill Lowry was instrumental in advancing this research project, and was always generous with his time and good advice. Professor Kathrin Plath was also a close collaborator, and played an essential role in this project.

I really appreciate the scientific discussions and support of the members of the Christofk lab. Undergraduate researcher Alanna Chan and I tilted at our share of windmills together, and not for a moment would I have rather been there with anybody else. Dr. Candice Hong, my bay-

mate for six years, was always encouraging and good at sharing. I want to thank Abby Krall for taking care of my cells on the weekends I was away. Lab helper, Margarita Calderon, and technicians, Adrian Garcia, Ethan Ahler, Carolina Espindola, and Katie Machado provided impeccable support for my daily work. Drs. Daniel Braas and Minh Thai taught me many techniques and provided constructive criticisms of my research. It was a great pleasure to work with graduate students Shivani Thaker and BJ Sullivan, clinical fellow Dr. James Ch'ng, undergraduate students Lisa Situ and Taylor Brown, and my office-mate Dr. Costos Chronis.

I could not have finished this thesis without my collaborators: Dr. Xavier Gaeta conducted neural differentiation-related experiments; Anna Sahakyan and Dr. Rachel Kim generated naive human embryonic stem cells; Dr. Rachel Kim also conducted human blastocyst staining; Jennifer Tsoi processed microarray data and helped with gene set enrichment analysis; Dr. Jin Zhang helped with oxygen consumption measurements; Dr. Ziwei Li helped with primed human embryonic stem cell culture; Jessica Cinkornpumin helped with RNA extraction; Angelyn Nguyen helped with microfluidic nuclear stiffness assay; Jinghua Tang cultured and expanded many human embryonic stem cell lines; Dr. John Lee generously shared important reagents with us; Ji Zhao and Keqian Wang designed and illustrated the cover for our story appeared in the journal *Cell Stem Cell*.

I owe a great deal to Dr. Yanyi Huang, who took me into his lab as an undergraduate student back at Peking University, and introduced science to me in a best possible way, with his charisma and conviction. Thanks to Dr. Xin Liu, who interviewed me for UCLA Pharmacology graduate program, and believed in me. I did my first lab rotation with Dr. Hsian-Rong Tseng at UCLA and he went out of his way to help me succeed. At UCLA, I was also fortunate to learn from Dr. Hong Wu, who is a brilliant cancer biologist.

I would like to thank my mom, Dr. Huaying Feng, for being an inspiration for me to pursue this degree. When I was eight year old, she juggled pursuing a PhD in Russian Literature and taking care of me in a dorm room shared with another graduate student. I very much appreciate my maternal grandmother, Yuanzhen Qian, who was also my first-grade Chinese teacher, for taking care of me for a whole year.

I also want to thank my dad, Dr. Kaihua Gu, for being a steadying influence in my life, and my uncle's family, Minfang Wang, Kaimin Gu, and Yuexiao Gu, for making me feel special when I grew up, and my paternal grandmother, Yong'e Yang, for taking care of me when I was in elementary school and later in high school.

I am very grateful to my girlfriend, Chi Zhang for being the person in my life who is compassionate, understanding, and always excited for new things. And a graceful skater on ice.

Maxime Chapon has been everything I could ask of a roommate. In particular, thanks for going to gym with me, and many thought-provoking discussions. I want to thank my graduate school friends who celebrated many birthdays and holidays with me: Dr. Gayle Boxx, Wing Lung, Dr. Andrew Pati Ah Young, Dr. Anna Reichardt, Dr. Pop Wongpalee, Dr. Lotus Loo, Ji Zhao, Di Cui, Kika Wenxi Wei, Yen San Michelle Lo, Elizabeth Xiwen Miao, Kikuye Ouchida, Joseph Hargan Calvopina, Johnathan Nakashima, Jessica Kim, Stacey Chiong, Dominique Lisiero, Autumn York, Jerry Villa, Kathi Wenz, Evan Sonntag, Bobby Guerra, Matthew Gonzales, Dr. Nae Chantaravisoot, Dr. Yan Song, Joann Zhuoyuan Lu, Dr. Maomeng Tong, Dr. Xin Rong, Dr. Yitong Zhao, Dr. Melissa McCracken, and Dr. Chelsea Robertson. My largest debt of gratitude is to the many families in Los Angeles who kindly invited me over for holidays

and dinners: Caryn Hoffman, the Deer family, the Hong family, Claire Cui and Jason Peng, the Jen family, the Badener family, and Dr. Yubin Dai's family.

I was also fortunate to spend two years with UCLA Outdoor Adventures. I particularly admired the program coordinator Roddy McCalley, for his teaching skills, integrity, passion for outdoor education, and sharing of poetry. I had many precious memories from the rivers, mountains, deserts, and hot springs of California, with Colin Ho, Brent Kennis, Kajori Purkayastha, Anna George, Jenny and Erik Knall, Mike Lavell, Julia Martinez, Emili Cardenas, Drew Preedeedilok, Dillon Green, Claire Cutler, Emma Wisdom, Ryo Stone, Thomas Arndt, Jessa Culver, Ermi Miao, Ari Migdale, Greg Senning, Rachel Davidson, Hannah Aldern, Dylan Chouinard, Grant Guess, Kaitlin Highstreet, Tommaso Bulfone, Abby MacPhee, Travis Cohantz, Mike Homer, Emma Lidington, Montana Marshall, Laura McNerny, April McGuire, Chris Millbern, Kaela Nye, Matt Rich, Billy Vainer, Chris Whitesides, Kelsey Wittles, Rita Neat, Nicole Pepper, Conor Cusack, Cory McClintic, Eva Wilson, Karen Bryan, Lisa Ciuffetti, Brandon Chau, Hannah Palmer, Katy Chappaz, Waldo Pritchard, Liz Bernier, Michelle Perrault, Paul Chen, and the late Sam Oliver, last of whom was often heard on a trip saying, "There's no place else I'd rather be."

I appreciate the support of California Institute for Regenerative Medicine Training Grant (TG2-01169) and UCLA Dissertation Year Fellowship for funding my research.

The work for this dissertation was performed under the direction of Dr. Heather Christofk.

Chapter 1

This chapter is based upon work from the manuscript

Gu, W., Gaeta, X., Sahakyan, A., Chan, A.B., Hong, C.S., Kim, R., Braas, D., Plath, K., Lowry, W.E. & Christofk, H.R. (2016). Glycolytic metabolism plays a functional role in regulating human pluripotent stem cell state. *Cell Stem Cell* 19, 476-490.

Chapter 2

This chapter is based upon work from the manuscript

Gu, W., Gaeta, X., Sahakyan, A., Chan, A.B., Hong, C.S., Kim, R., Braas, D., Plath, K., Lowry, W.E. & Christofk, H.R. (2016). Glycolytic metabolism plays a functional role in regulating human pluripotent stem cell state. *Cell Stem Cell* 19, 476-490.

Chapter 3

This chapter is based upon work from the manuscript

Gu, W., Gaeta, X., Sahakyan, A., Chan, A.B., Hong, C.S., Kim, R., Braas, D., Plath, K., Lowry, W.E. & Christofk, H.R. (2016). Glycolytic metabolism plays a functional role in regulating human pluripotent stem cell state. *Cell Stem Cell* 19, 476-490.

VITA

Education

Peking University, M.D., Preventive Medicine, 2009

Academic Employment

Graduate Student Researcher, Laboratory of Dr. Heather Christofk, UCLA, 2010 - 2017

Research Assistant, Laboratory of Dr. Yanyi Huang, Peking University, 2006 - 2009

Publications

Hong, C.S., Graham, N.A., Gu, W., Espindola Camacho, C., Mah, V., Maresh, E.L., Alavi, M., Bagryanova, L., Krotee, P.A.L., Gardner, B.K., et al. (2016). MCT1 Modulates Cancer Cell Pyruvate Export and Growth of Tumors that Co-express MCT1 and MCT4. *Cell Reports* 14, 1590–1601.

Gu, W., Gaeta, X., Sahakyan, A., Chan, A.B., Hong, C.S., Kim, R., Braas, D., Plath, K., Lowry, W.E. & Christofk, H.R. (2016). Glycolytic metabolism plays a functional role in regulating human pluripotent stem cell state. *Cell Stem Cell* 19, 476-490.

Invited Talks

2017	Keystone Symposia: Transcriptional and Epigenetic Control in Stem Cells, Olympic Valley, CA
2016	UCLA Biological Chemistry Monday Seminar Series, Los Angeles, CA
2016	UCLA Biomedical Research Minor 5HA (guest lecture), Los Angeles, CA
2014	UCLA Metabolism Interest Group, Los Angeles, CA

2014	UCLA Stem Cell Club, Los Angeles, CA
2012, 2013, 2015	UCLA Pharmacology Floor Meeting, Los Angeles, CA
2012, 2014, 2016	UCLA Pharmacology Retreat, Huntington Beach, CA

Honors and Awards

2016	Keystone Symposia Future of Science Fund Scholarship
2016	Dissertation Year Fellowship, UCLA Graduate Division
2015	Best Poster Presentation, UCLA Pharmacology Retreat
2013	Training Grant, California Institute for Regenerative Medicine
2008, 2009	International Summer Program Award, Tokyo Medical and Dental University
2007	Academic Excellence Award, Peking University
2005, 2006, 2008	Outstanding Medical Student, Peking University

CHAPTER 1. Human embryonic stem cells with a higher degree of pluripotency exhibit increased glycolysis

Introduction

Human embryonic stem cells (hESCs) can be derived from a region of the human embryo called the inner cell mass at the early blastocyst stage of development (5 days post-fertilization). They hold great promise in regenerative medicine and can be used as a model for studying human embryology, because they possess two remarkable characteristics: pluripotency and self-renewal. Pluripotency is their potential to differentiate into all cell types of the adult body, such as neurons, hepatocytes, and blood cells; self-renewal is their ability to remain pluripotent and undifferentiated while replicating themselves *in vitro*.

Glucose is of central importance in the cellular metabolism of mammalian animals, and plays an important role in both catabolic and anabolic metabolism. An excellent source of energy, glucose produces 2,840 kJ/mol upon its complete oxidation to carbon dioxide and water in mitochondria. On the anabolic side, intermediates of glucose metabolism are responsible for the synthesis of numerous molecules required for cellular biology, including amino acids, fatty acids, nucleotides, and coenzymes. Glycolysis, the central pathway of glucose metabolism, metabolizes one molecule of glucose, a six-carbon compound, through a series of enzyme-catalyzed reactions, to produce two molecules of three-carbon compound pyruvate. Glycolysis releases free energy from glucose, which is stored in the form of ATP and NADH. More importantly, through many bifurcating pathways, namely the pentose phosphate pathway, serine synthesis pathway, citric acid cycle etc., glycolysis produces important intermediates for the synthesis of macromolecules, which are essential building blocks for proliferating cells.

An association between glycolysis and pluripotency is well-established (Folmes et al., 2013, 2012a, 2012b; Zhang et al., 2011, 2012). Cultured pluripotent human embryonic stem cells (hESCs) exhibit high rates of glycolysis that diminish upon differentiation (Chung et al.,

2010; Prigione et al., 2010). Additionally, somatic cells exhibit increased glycolysis and decreased respiration upon reprogramming into pluripotent stem cells (Folmes et al., 2013, 2011; Zhang et al., 2012). However, the role of glycolytic metabolism in the ability of hESCs to undergo self-renewal or differentiation is not well understood.

Recently several methods have been developed to allow for a conversion from the typical hESC state of pluripotency to a more naive state, akin to that found in mouse ESCs (Chan et al., 2013; Gafni et al., 2013; Takashima et al., 2014; Theunissen et al., 2014; Valamehr et al., 2014; Ware et al., 2014). Conventional hESCs, now considered to be in the primed pluripotent state, share molecular and functional properties with epiblast stem cells as described in mouse development, whereas naive hESCs are thought to better represent cells found in the inner cell mass of an embryo (Gafni et al., 2013; Theunissen et al., 2014; Ware et al., 2014). Culturing of naive hESCs represent a major advance to regenerative medicine since the ability to produce "clones" of human pluripotent stem cells is severely hampered in primed hESCs and induced pluripotent stem cells (hiPSCs), limiting the opportunities to perform genomic manipulation by homologous recombination or CRISPR/Cas systems. The naive state of pluripotency is defined by expression of a specific set of pluripotency genes, genome-wide chromatin changes such as DNA hypomethylation, and the ability to survive plating at clonal density. While extensive effort has established the metabolic state of primed hESCs as characterized by enhanced glycolysis and decreased respiration, the metabolic state of naive cells remains less well understood. Recently Takashima et al. showed induction of oxidative phosphorylation pathways and changes in mitochondrial depolarization in human naive cells (Takashima et al., 2014), and Sperber et al. demonstrated naive and primed cells differ significantly in their metabolome, affecting their epigenetic landscapes (Sperber et al., 2015), but neither specifically measured

glycolytic rate, utilization of glucose molecules, or the regulation of glycolysis in naive hESCs. Further characterization of naive cell metabolism may reveal additional defining characteristics of the naive state and improve our understanding of the links between metabolism and pluripotency. Here we investigate glucose metabolism in naive versus primed hESCs, and the regulation of glycolytic metabolism in human pluripotency. In so doing, we make important insights about the metabolism of cells at different stages of pluripotency.

Results

hESCs with a higher degree of pluripotency exhibit increased glycolysis

Consistent with an association between glycolytic metabolism and the pluripotent state (Folmes et al., 2012b; Varum et al., 2011), we found that retinoic acid-induced differentiation of primed hESCs results in decreased glucose consumption, decreased lactate production (Figure 1-1), and increased oxygen consumption rates (Figure 1-2). These results suggest a shift away from glycolytic metabolism and towards oxidative metabolism during retinoic acid-induced differentiation of hESCs into the three primordial germ layers.

Since glycolytic metabolism is associated with the pluripotent state, we hypothesized that glycolytic rate may vary across human stem cells with different degrees of pluripotency. To determine whether conversion of primed hESCs to the naive pluripotent state impacts glycolytic rate, we induced primed hESC lines UCLA1 and UCLA9 to a naive state by the 5i/LAF method (Pastor et al., 2016; Theunissen et al., 2014). Sub-clones of naive cells were isolated, and the metabolism of these naive cells was compared to the primed hESCs from which they were derived. Notably, both clones of naive UCLA1 and naive UCLA9 hESCs exhibit higher glucose consumption and lactate production rates (Figures 1-3 and 1-4) than the primed cells from which they were derived. Importantly, primed UCLA9 hESCs placed in naive medium for 24 hours do not exhibit increased glycolytic rates (Figure 1-3), suggesting that the increased glycolytic rates in naive hESCs are associated with acquisition of naive cell identity, and not due to the factor(s) in naive media. To further examine whether increased glycolytic rate is associated with naive pluripotency, we derived a naive cell line directly from the inner cell mass of a human blastocyst in 5i/LAF medium. In this naive line that was never exposed to primed culture conditions, we also found increased glucose consumption and lactate production rates relative to two primed

hESC lines (Figure 1-5). Additionally, we found that naive/reset hESCs derived using the Takashima et al. method (Takashima et al., 2014) exhibit increased glycolytic rates compared to the primed hESCs from which they were derived (Figure 1-6). Consistent with the induction of the naive state by Takashima et al. we also observed an increase in oxygen consumption in our 5i/LAF induced naive lines compared to their primed counterparts (Figure 1-7). These results support a strong association between glycolytic metabolism and pluripotency and suggest that modulation of glucose metabolism may be involved in the acquisition of naive state.

To further characterize how the glucose metabolism of naive hESCs differs from that of primed cells, we labeled UCLA1 and UCLA9 naive and primed hESCs with 1,2-^{13}C-glucose and traced the incorporation of ^{13}C into downstream glucose metabolites using liquid chromatography-mass spectrometry (LC-MS). Consistent with elevated glycolytic flux in naive hESCs, we found increased ^{13}C incorporation into lactate (Figure 1-8) and increased levels of most glycolytic intermediates (Figure 1-9). This suggested that the increased glycolysis observed in naive hESCs is associated with acquisition of naive cell identity, and was not a result of factor(s) in the media used to derive the naive hESCs. Notably, we also found that naive hESCs derived from two different hESC lines, UCLA1 and UCLA9, incorporate more glucose carbons into purine and pyrimidine nucleotides (Figure 1-10). The increased M1 isotopologues of nucleotides from naive hESCs labeled with 1,2-^{13}C-glucose suggests increased flux through the oxidative pentose phosphate pathway in naive versus primed hESCs (Figures 1-11 and 1-9). Additionally, we found that UCLA1 and UCLA9 naive hESCs incorporate more glucose carbons into serine than primed hESCs (Figure 1-12), an important metabolite for one-carbon metabolism and purine and glutathione biosynthesis (Locasale, 2013). Unlike naive hESCs, primed UCLA9 hESCs placed in naive cell medium for 24 hours do not exhibit increased ^{13}C-labeling of

nucleotides and serine (Figures 1-10 and 1-12). Collectively, these results suggest that acquisition of the naive state is accompanied by a further increase glucose metabolism and the use of glucose to generate nucleotides and serine.

N-MYC is associated with human naive pluripotency

Given our data that the metabolic phenotype of naive cells is characterized by increased glucose metabolism, we next performed gene set enrichment analysis (GSEA) (Subramanian et al., 2005) on RNA-Seq data from the primed hESCs versus naive cell clones to identify metabolism-related gene sets distinct between these two state of pluripotency. We found that MYC-regulated gene sets are significantly enriched in naive versus primed cells (Figures 1-13 and 1-14). To test whether this enrichment applies to other naive conditions than the 5i/LAF method, we analyzed previously published human blastocyst datasets (Vassena et al., 2011; Yan et al., 2013) and another naive hESC dataset by Takashima et al. (Takashima et al., 2014). We first noticed the expression patterns in KEGG glycolysis pathway genes are very similar between naive hESCs derived by Takashima et al. and those derived using the 5i/LAF method when compared to their respective primed counterparts (Figures 1-15 and 1-16). More importantly, in multiple independent studies, we found that MYC target genes are enriched in blastocyst versus primed hESCs (Figure 1-17), and in another naive line versus its primed counterpart (Figure 1-18), suggesting that elevated MCY target gene expression is not unique to 5i/LAF-derived naive cells, but is a characteristic of naive pluripotency *in vivo* and likely other naive culture conditions as well. This is notable since MYC can promote increased glucose metabolism and is associated with the pluripotent sate (Takahashi and Yamanaka, 2006; Thai et al., 2014).

Consistent with an association between MYC activity and pluripotency, we found that nuclear N-MYC and C-MYC levels are decreased upon retinoic acid-induced differentiation of primed hESCs (Figure 1-19), while two independently derived naive clones exhibit higher nuclear N-MYC and C-MYC levels than the primed cells from which they were derived (Figure 1-20). We confirmed the increased N-MYC and C-MYC levels in naive versus primed hESCs by immunofluorescence staining, which additionally shows differences in sub-nuclear localization of N-MYC: dispersive nuclear N-MYC signal in naive cells, and contained nucleolar N-MYC staining in primed cells (Figure 1-21). To test whether the elevated nuclear N-MYC levels we detected in 5i/LAF-derived naive hESCs reflect that of naive pluripotency *in vivo*, we examined N-MYC and C-MYC levels by immunofluorescence in human blastocysts, and found increased nuclear N-MYC signal in the inner cell mass relative to that found in trophoblasts (Figure 1-22). In contrast, we readily detected nuclear C-MYC signal in both the inner cell mass and trophoblasts, suggesting N-MYC may be more specifically associated with naive pluripotency than C-MYC. Given the enrichment of MYC target gene expression and elevation of nuclear N-MYC levels in naive versus primed hESCs, we postulated that N-MYC activity might be important for the maintenance of naive pluripotency. Consistent with this notion, we found that treatment with CD532, a small molecule inhibitor towards N-MYC (Gustafson et al., 2014), dramatically decreases the proliferation of naive hESCs without affecting the proliferation of primed hESCs (Figure 1-23), suggesting an important role for N-MYC specifically in naive hESCs. These results further suggest an association between MYC activity, glucose metabolism, and the pluripotent state.

Discussion

This study confirms previous findings that glycolytic metabolism is associated with the pluripotent state, and extends them significantly to the naive state. We show that acquisition of a naive state further increases hESC glycolysis, and that retinoic acid-induced differentiation decreases glycolytic metabolism (Figure 1-24). The elevated glycolytic metabolism in naive hESCs is accompanied by increased MYC transcriptional activity and increased nuclear N-MYC and C-MYC levels. While C-MYC has previously been associated with pluripotency and has been used to enhance reprogramming of somatic cells into induced pluripotent stem cells (Smith et al., 2010; Takahashi and Yamanaka, 2006), N-MYC has been less studied in hESCs and may be an important contributor to pluripotency-associated glycolytic metabolism.

Through LC-MS-based metabolomics, we show that naive hESCs incorporate more glucose carbons into lactate, nucleotides, and serine. Since naive hESCs are thought to be more representative of the inner cell mass of the preimplantation embryo than primed hESCs, which are thought to resemble the post-implantation epiblast (Nichols and Smith, 2009), we hypothesize that variation in nutrient availability to the embryo before and after implantation may contribute to the differences in metabolism between the naive and primed state. Consistent with this notion, we found that MYC target genes are enriched in human embryos at the morula and blastocyst stages relative to hESCs (Figure 1-17 and Vassena et al., 2011), suggesting that our cultured naive hESCs, which also show enrichment of MYC target genes, may best represent cells from the morula and blastocyst stages.

The increased glycolytic rate we show in human naive versus primed hESCs is different from the glucose metabolism found in mouse naive versus primed ESCs (mESCs versus Epiblast Stem Cells (EpiSCs), respectively). mESCs exhibit lower glycolytic rates compared to mEpiSCs

(Zhou et al., 2012 and Figure 1-25). This discrepancy may be partially explained by the lower nuclear C-MYC levels in mESCs versus mEpiSCs (Marks et al., 2012 and Figure 1-26). In human, the opposite is true: naive hESCs have higher nuclear C-MYC levels than primed hESCs (Figure 1-20). Of late, there is emerging literature on the differences in early embryo development between human and mouse: lineage and X chromosome dynamics (Petropoulos et al., 2016), dependence on FGF signaling (Roode et al., 2012), and gene expression patterns (Niakan and Eggan, 2013). Considering our key observations regarding glycolysis in naive hESCs holds true in a naive line directly derived from a human blastocyst, and were corroborated by MYC gene expression studies and immunofluorescence staining in human blastocysts, our results suggest the regulation of glycolytic metabolism may be yet another key aspect of the human-mouse difference during early embryo development.

Figures

Figure 1-1

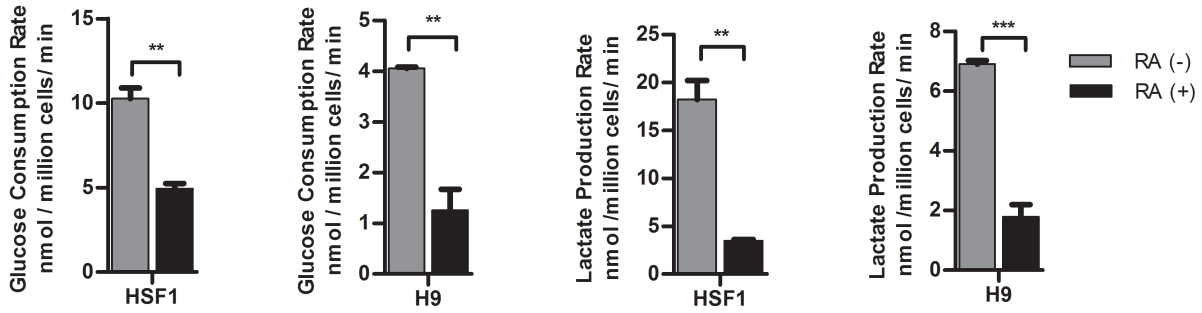

Retinoic acid-induced differentiation of primed hESCs results in decreased glucose consumption and decreased lactate production. Glucose consumption rates (left and center left) and lactate production rates (center right and right) of primed HSF1 and H9 hESCs treated for 7 days with DMSO (RA (-)) or 10 μM retinoic acid (RA (+)). Error bars indicate ± 1 SEM of biological replicates (n = 3). ** $p < 0.01$; *** $p < 0.001$.

Figure 1-2

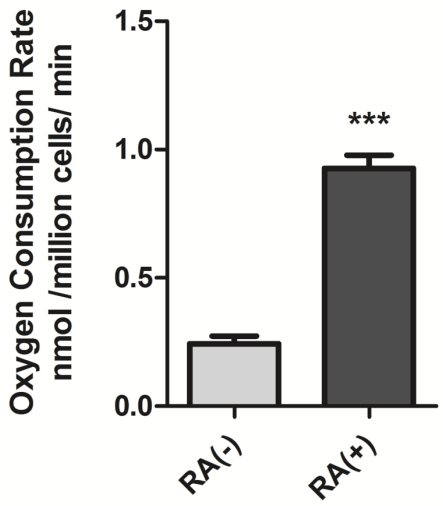

Retinoic acid-induced differentiation of primed hESCs causes increased oxygen consumption rates. Oxygen consumption rates in FS HSF1 hESCs, treated for 7 days with DMSO (RA (-)) or 10 μM retinoic acid (RA (+)), as measured by an anaerobic chamber fitted with a fiber optic oxygen sensor. Error bars indicate ± 1 SEM of biological replicates (n = 3). *** $p < 0.001$.

Figure 1-3

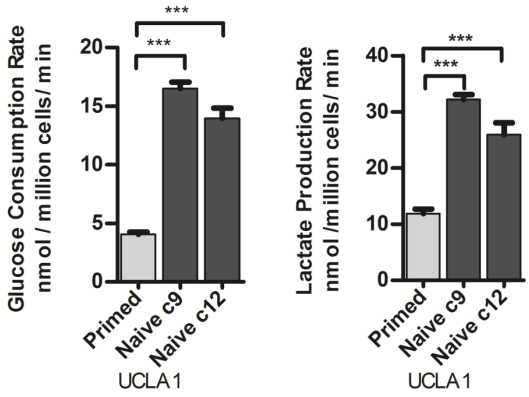

Both clones of naive UCLA1 exhibit higher glucose consumption and lactate production rates than the primed cells from which they were derived. Glucose consumption rates (left) and lactate production rates (right) of primed UCLA1 hESCs and naive UCLA1 hESC clone 9 and clone 12 generated by the 5i/LAF method. Error bars indicate ± 1 SEM of biological replicates (n = 3). *** $p < 0.001$.

Figure 1-4

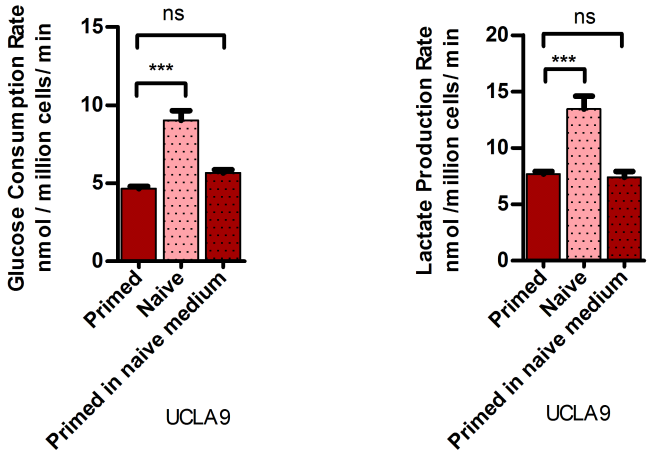

UCLA9 hESCs exhibit higher glucose consumption and lactate production rates than the primed cells from which they were derived. Glucose consumption (left) and lactate production (right) rates of primed UCLA9 hESCs, naive UCLA9 hESCs generated by the 5i/LAF method, and primed UCLA9 hESCs placed in naive cell medium for 24 hours. Error bars indicate ± 1 SEM of biological replicates (n = 3). ns: not significant; *** $p < 0.001$.

Figure 1-5

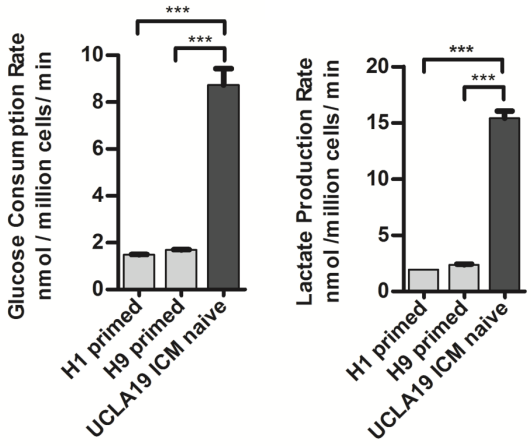

A naive cell line derived directly from the inner cell mass of a human blastocyst exhibits increased glucose consumption and lactate production rates relative to two primed hESC lines. Glucose consumption rates (left) and lactate production rates (right) of primed H1 and H9 hESCs, and naive UCLA19 hESCs derived from the inner cell mass of a human blastocyst and cultured in 5i/LAF medium. Error bars indicate ± 1 SEM of biological replicates (n = 3). *** $p < 0.001$.

Figure 1-6

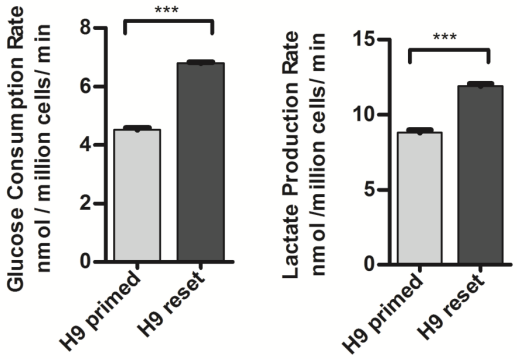

Naive/reset hESCs derived using the Takashima et al. method exhibit increased glycolytic rates compared to the primed hESCs from which they were derived. Glucose consumption rates (left) and lactate production rates (right) of primed H9 hESCs and naive/reset H9 hESCs generated by the Takashima et al. method (Takashima et al., 2014). Error bars indicate ± 1 SEM of biological replicates (n = 3). *** $p < 0.001$.

Figure 1-7

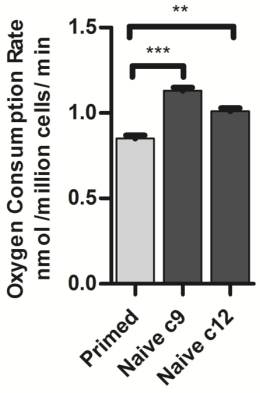

5i/LAF induced naive lines exhibit an increase in oxygen consumption compared to their primed counterparts. Oxygen consumption rates of primed UCLA1 hESCs and naive UCLA1 hESC clone 9 and clone 12 generated by the 5i/LAF method. Error bars indicate ± 1 SEM of biological replicates (n = 3** $p < 0.01$; *** $p < 0.001$.

Figure 1-8

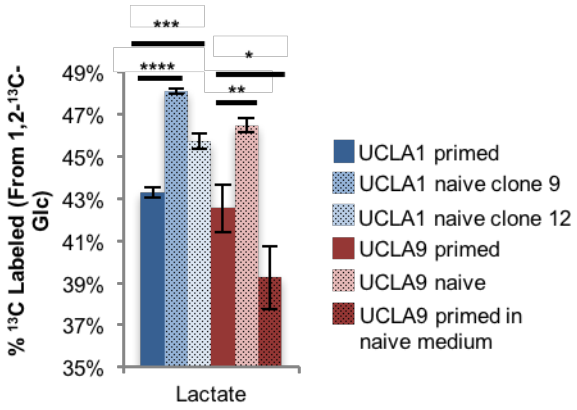

Naive hESCs exhibit increased ^{13}C incorporation from 1,2-^{13}C-glucose into lactate.

Percentages of ^{13}C-labeled lactate extracted from the indicated cells. Primed UCLA1 hESCs, naive UCLA1 hESC clone 9 and clone 12, and primed UCLA9 hESCs, naive UCLA9 hESC, and primed UCLA9 hESCs placed in naive cell medium, were cultured in medium containing 1,2-^{13}C-glucose for 24 hours prior to metabolite extraction and analysis by LC-MS. Error bars indicate ± 1 SEM of biological replicates (n = 3). * $p < 0.05$; ** $p < 0.01$; *** $p < 0.001$.

Figure 1-9

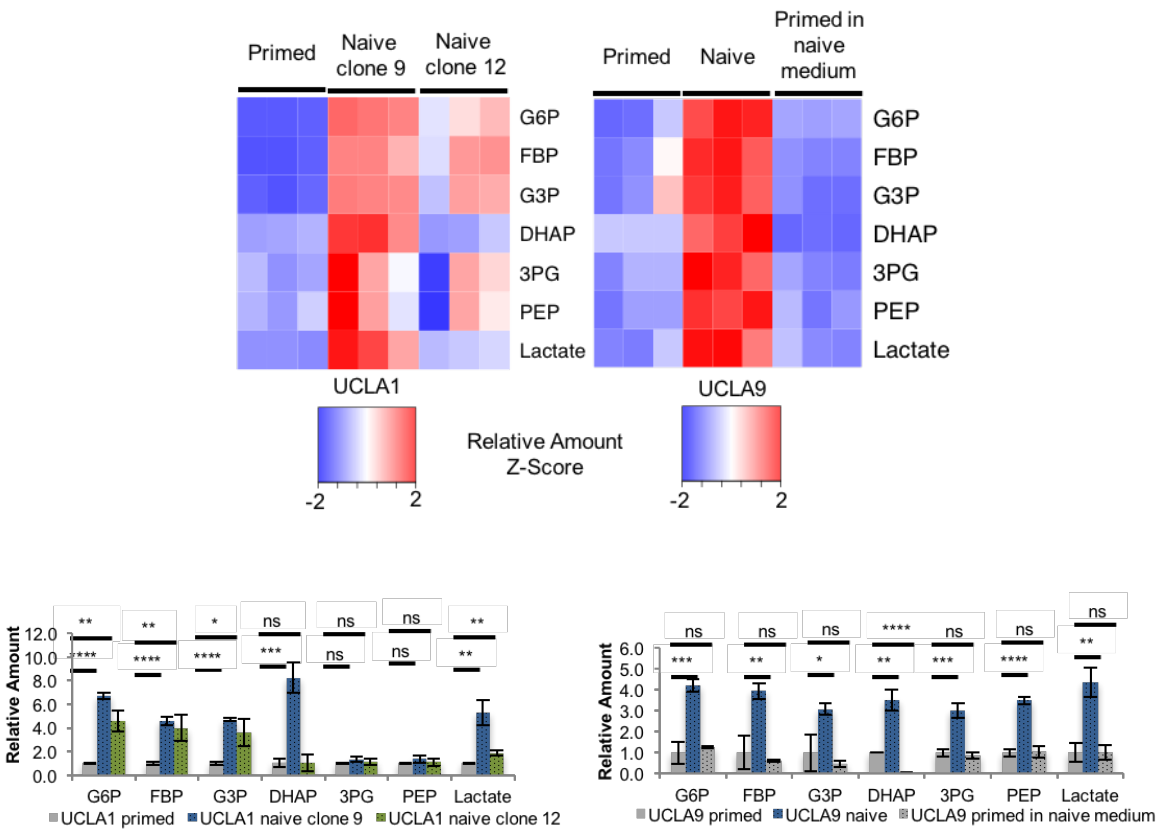

(legend on next page)

Naive hESCs exhibit increased levels of most glycolytic intermediates. Heatmap (top) and bar graphs (bottom) showing relative amounts of glycolytic intermediates, glucose-6-phosphate (G6P), fructose bisphosphate (FBP), glyceraldehyde-3-phosphate (G3P), dihydroxyacetone phosphate (DHAP), 3-phosphoglycerate (3PG), phosphoenolpyruvate (PEP), and lactate, from the indicated cells. The heatmap shows standardized amounts of indicated metabolites across samples (Z score). Primed UCLA1 hESCs, naive UCLA1 hESC clone 9 and clone 12, and primed UCLA9 hESCs, naive UCLA9 hESC, and primed UCLA9 hESCs placed in naive cell medium, were cultured in medium containing 1,2-^{13}C-glucose for 24 hours prior to metabolite extraction and analysis by LC-MS. Error bars indicate ± 1 SEM of biological replicates (n = 3). ns: not significant; * $p < 0.05$; ** $p < 0.01$; *** $p < 0.001$; **** $p < 0.0001$.

Figure 1-10

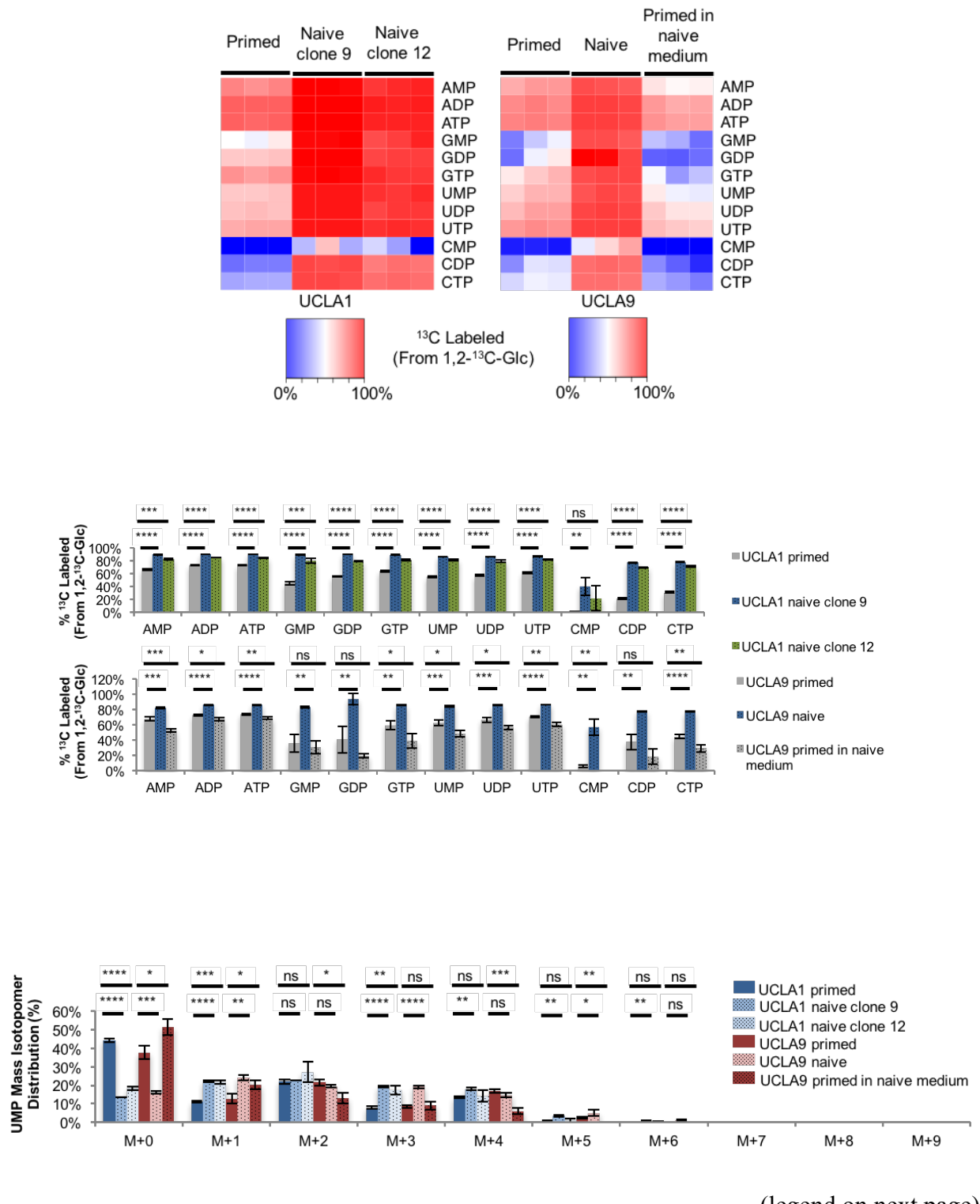

(legend on next page)

Naive hESCs incorporate more glucose carbons into purine and pyrimidine nucleotides. Heatmap (top) and bar graphs (middle) showing percentages of ^{13}C- labeled nucleotides extracted from the indicated cells, and bar graphs (bottom) showing mass isotopomer distribution of the indicated ^{13}C- labeled UMP extracted from the indicated cells. Primed UCLA1 hESCs, naive UCLA1 hESC clone 9 and clone 12, and primed UCLA9 hESCs, naive UCLA9 hESC, and primed UCLA9 hESCs placed in naive cell medium, were cultured in medium containing 1,2-^{13}C-glucose for 24 hours prior to metabolite extraction and analysis by LC-MS. Error bars indicate ± 1 SEM of biological replicates (n = 3). ns: not significant; * $p < 0.05$; ** $p < 0.01$; *** $p < 0.001$; **** $p < 0.0001$.

Figure 1-11

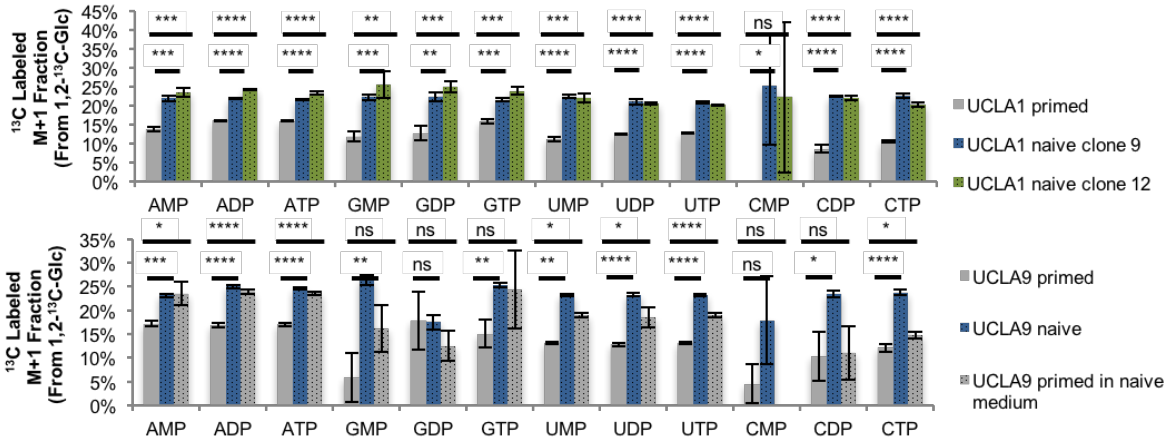

Increased M1 isotopologues of nucleotides from naive hESCs labeled with 1,2-^{13}C-glucose versus primed hESCs. Percentages of the indicated ^{13}C-labeled M+1 form of nucleotides extracted from the indicated cells. Primed UCLA1 hESCs, naive UCLA1 hESC clone 9 and clone 12, and primed UCLA9 hESCs, naive UCLA9 hESC, and primed UCLA9 hESCs placed in naive cell medium, were cultured in medium containing 1,2-^{13}C-glucose for 24 hours prior to metabolite extraction and analysis by LC-MS. Error bars indicate ± 1 SEM of biological replicates (n = 3). ns: not significant; * $p < 0.05$; ** $p < 0.01$; *** $p < 0.001$; **** $p < 0.0001$.

Figure 1-12

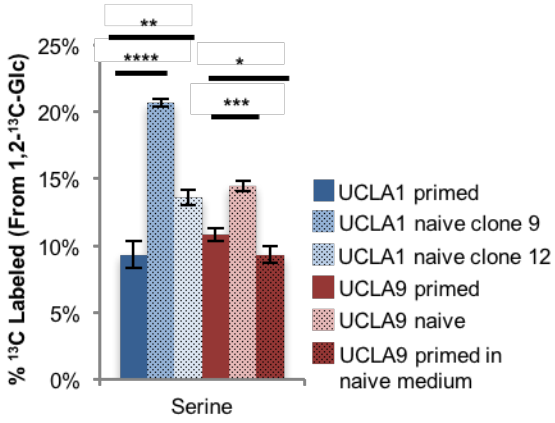

Naive hESCs incorporate more glucose carbons into serine than primed hESCs.

Percentages of ^{13}C-labeled serine extracted from the indicated cells. Primed UCLA1 hESCs, naive UCLA1 hESC clone 9 and clone 12, and primed UCLA9 hESCs, naive UCLA9 hESC, and primed UCLA9 hESCs placed in naive cell medium, were cultured in medium containing 1,2-^{13}C-glucose for 24 hours prior to metabolite extraction and analysis by LC-MS. Error bars indicate ± 1 SEM of biological replicates (n = 3). * $p < 0.05$; ** $p < 0.01$; *** $p < 0.001$.

Figure 1-13

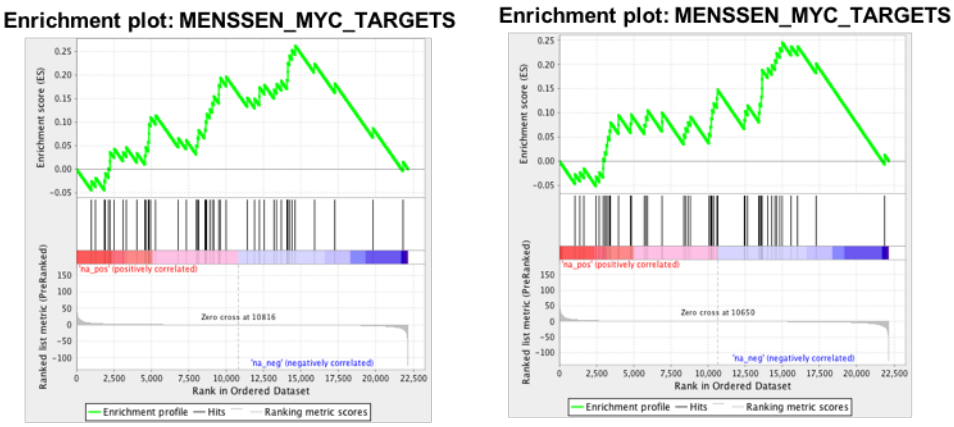

UCLA1 naive c9 versus UCLA1 primed
ES = 0.262, NES = 2.18
p < 0.001, FDR = 0.0163

UCLA1 naive c12 versus UCLA1 primed
ES = 0.246, NES = 2.06
p = 0.00196, FDR = 0.0277

MYC-regulated gene sets are significantly enriched in naive versus primed cells. GSEA mountain plots displaying enrichment of a MYC-regulated gene set in naive UCLA1 clone 9 (left) and naive UCLA1 clone 12 (right) versus primed UCLA1 hESCs.

Figure 1-14

MENSSEN_MYC_TARGETS

URL: http://software.broadinstitute.org/gsea/msigdb/cards/MENSSEN_MYC_TARGETS

> Genes up-regulated by adenoviral expression of c-MYC [GeneID=4609] in HUVEC cells (umbilical vein endothelium).

APEX1	EIF5AL1	HSPD1	MSH2	RPS19
BRCA1	ENO1	HSPE1	NCL	RRP9
C1QBP	EPRS	HSPH1	NME1	RUVBL2
CCNB1	FKBP4	KAT2B	NOP56	SCARB1
CCT3	HERC5	KIAA0664	NPM1	SLPI
CDK4	HNRPDL	LDHA	NSF	SRM
DDX21	HSP90AA1	LDHB	NUTF2	TRAP1
DNAJB1	HSP90AB1	METAP2	PFKM	TSPO
EFTUD2	HSPA1A	MGST1	PHB	YWHAE
EI24	HSPA8	MNT	POLR2F	
EIF3B	HSPA9	MRPL3	PPIF	

Members of the MYC target gene set by Menssen et al.

Figure 1-15

(legend on next page)

The expression patterns in KEGG glycolysis pathway genes are very similar between naive hESCs derived by Takashima et al. and those derived using the 5i/LAF method when compared to their respective primed counterparts. Cytoscape network map showing the fold change of KEGG glycolysis genes in naive UCLA1 hESC clone 9 versus primed UCLA1 hESCs (top left), naive UCLA1 hESC clone 12 versus primed UCLA1 hESCs (top right), and Takashima reset versus primed H9 hESCs (bottom). Genes in red indicate increased mRNA expression levels in naive or reset cells. Genes in green indicate increased mRNA expression levels in primed cells.

Figure 1-16

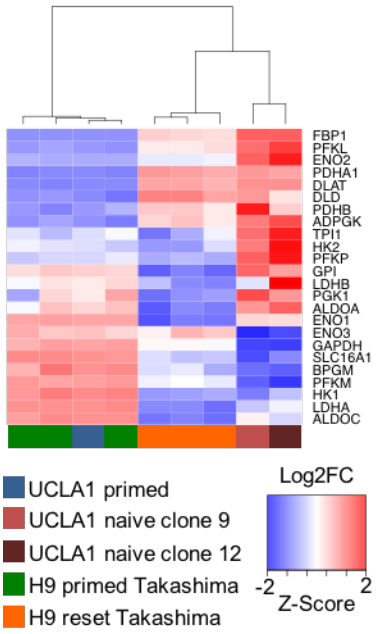

Clustering of naive hESCs derived by Takashima et al., naive hESCs derived using the 5i/LAF method, and their respective primed counterparts, according to their expression levels of KEGG glycolysis pathway genes. Heatmap depicting log2 fold changes of KEGG glycolysis genes across UCLA1 primed, UCLA1 naive clone 9 and clone 12, and Takashima reset and primed H9 hESCs. Bottom colored bars indicate sample origins.

Figure 1-17

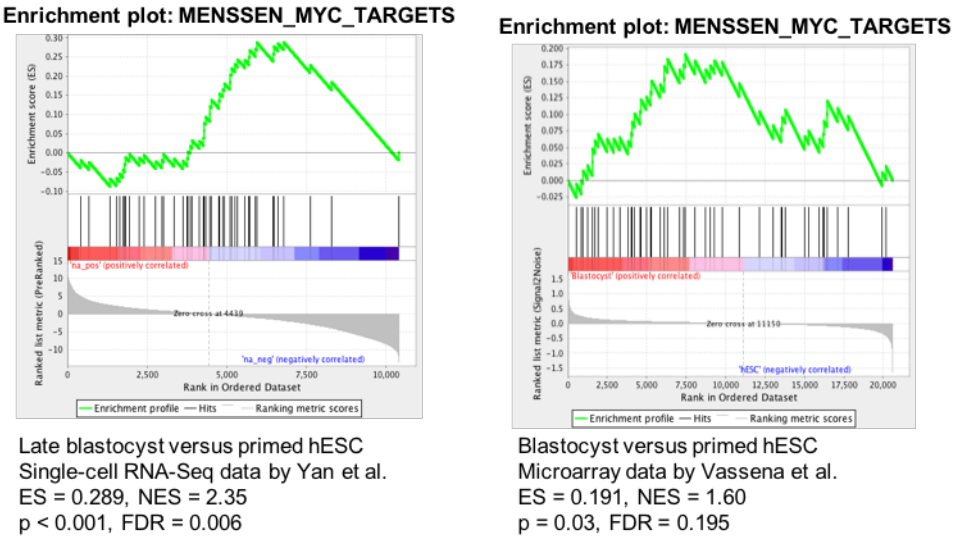

	Oocyte	2-cell	4-cell	6-cell	8 to 10-cell	Morula	Blastocyst	ESC
Oocyte vs	-	N.E.	0.77	N.E.	N.E.	N.E.	N.E.	N.E.
2-cell vs	0.89	-	1.52	N.E.	N.E.	N.E.	N.E.	N.E.
4-cell vs	N.E.	N.E.	-	N.E.	N.E.	N.E.	N.E.	N.E.
6-cell vs	1.33	1.07	1.72	-	N.E.	N.E.	N.E.	N.E.
8 to 10-cell vs	2.64	2.59	2.24	2.47	-	N.E.	N.E.	1.2
Morula vs	1.92	1.91	2.44	2.51	0.97	-	1.11	1.78
Blastocyst vs	2.29	2.01	2.13	2.58	0.98	N.E.	-	1.57
ESC vs	2.22	2.32	2.23	2.15	N.E.	N.E.	N.E.	-

N.E. = Not enriched

Normalized enrichment score

0.5 4.0

MYC target genes are enriched in blastocyst versus primed hESCs. GSEA mountain plots displaying enrichment of a MYC-regulated gene set in human late blastocyst versus primed hESCs (top left) using RNA-Seq data by Yan et al., 2013, and human blastocyst versus primed hESCs (top right) from mRNA microarray data by Vassena et al., 2011. Heatmap (bottom) showing the enrichment of MYC- regulated genes across various early human embryo development stages from Vassena et al. dataset. Each cell contains the normalized enrichment score (NES), based on GSEA, from pairwise comparison of two different cell types, as indicated. N.E.: not enriched.

Figure 1-18

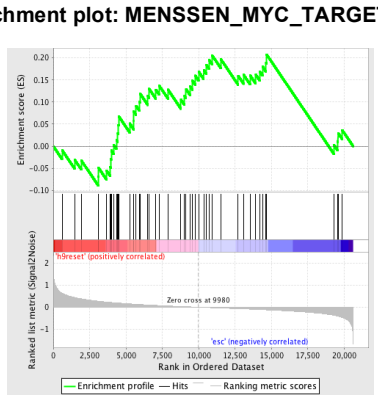

H9 reset versus primed hESCs
Microarray data by Takashima et al.
ES = 0.207, NES = 1.69
p = 0.030, FDR = 0.080

MYC target genes are enriched in a naive line derived by the Takashima et al. method versus its primed counterpart. GSEA mountain plot displaying enrichment of MYC-regulated genes in H9 reset versus primed hESCs.

Figure 1-19

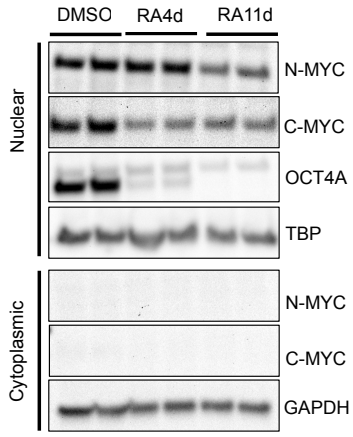

Nuclear N-MYC and C-MYC levels are decreased upon retinoic acid-induced differentiation of primed hESCs. Immunoblot showing nuclear and cytoplasmic N-MYC and C-MYC levels in primed feeder-free hESCs treated with DMSO, retinoic acid for 4 days (RA4d), or retinoic acid for 11 days (RA11d). Nuclear OCT4A levels are also shown. TBP is used as a loading control for the nuclear lysates. GAPDH is used as a loading control for the cytoplasmic lysates. Lysates were prepared in biological duplicates.

Figure 1-20

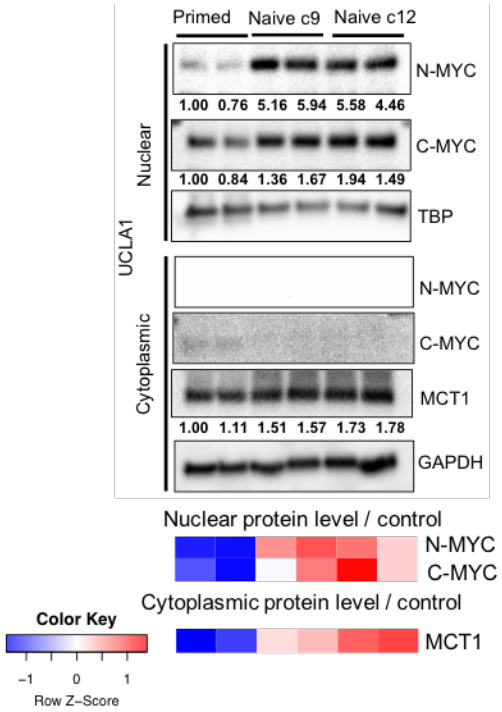

Naive hESCs exhibit higher nuclear N-MYC and C-MYC levels than the primed cells from which they were derived. Immunoblot showing nuclear and cytoplasmic N-MYC and C-MYC levels in primed, naive clone 9, and naive clone 12 UCLA1 hESCs. Cytoplasmic MCT1 levels are also shown. The heatmap shows standardized levels of indicated markers across samples (Z score). TBP is used as a loading control for the nuclear lysates. GAPDH is used as a loading control for the cytoplasmic lysates. Lysates were prepared in biological duplicates.

Figure 1-21

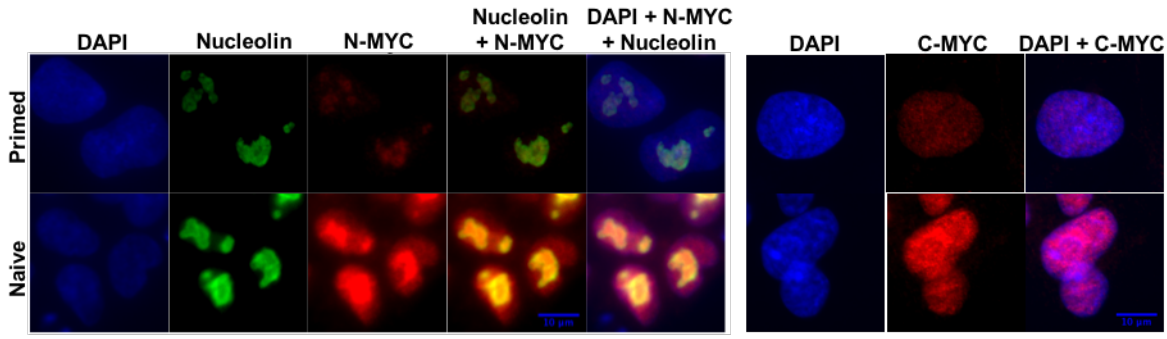

Increased N-MYC and C-MYC levels in naive versus primed hESCs and sub-nuclear localization of N-MYC. Immunofluorescence staining for N-MYC and C-MYC in naive versus primed UCLA1 hESCs. Nucleolin staining is also shown. Scale bar = 10μm.

Figure 1-22

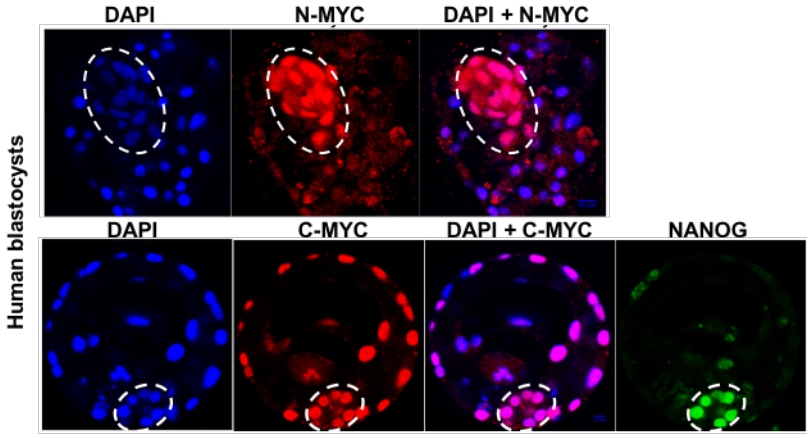

Increased nuclear N-MYC signal in the inner cell mass relative to that found in trophoblasts. Immunofluorescence staining for N-MYC and C-MYC in human blastocysts. The contour of inner cell mass is indicated by dashed line. NANOG staining is also shown. Scale bar = 10μm.

Figure 1-23

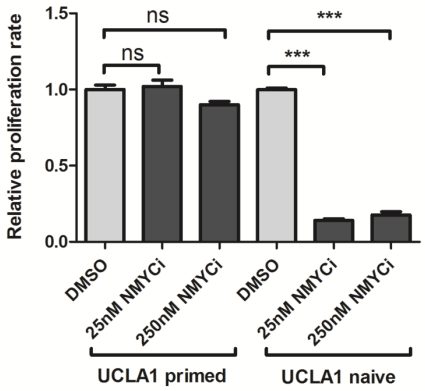

A small molecule inhibitor towards N-MYC dramatically decreases the proliferation of naive hESCs without affecting the proliferation of primed hESCs. Proliferation rates of primed versus naive feeder-supported UCLA1 hESCs treated with DMSO or 250 nM CD532 (NMYCi). Error bars indicate ± 1 SEM of biological replicates (n = 3). ns: not significant; *** $p < 0.001$.

Figure 1-24

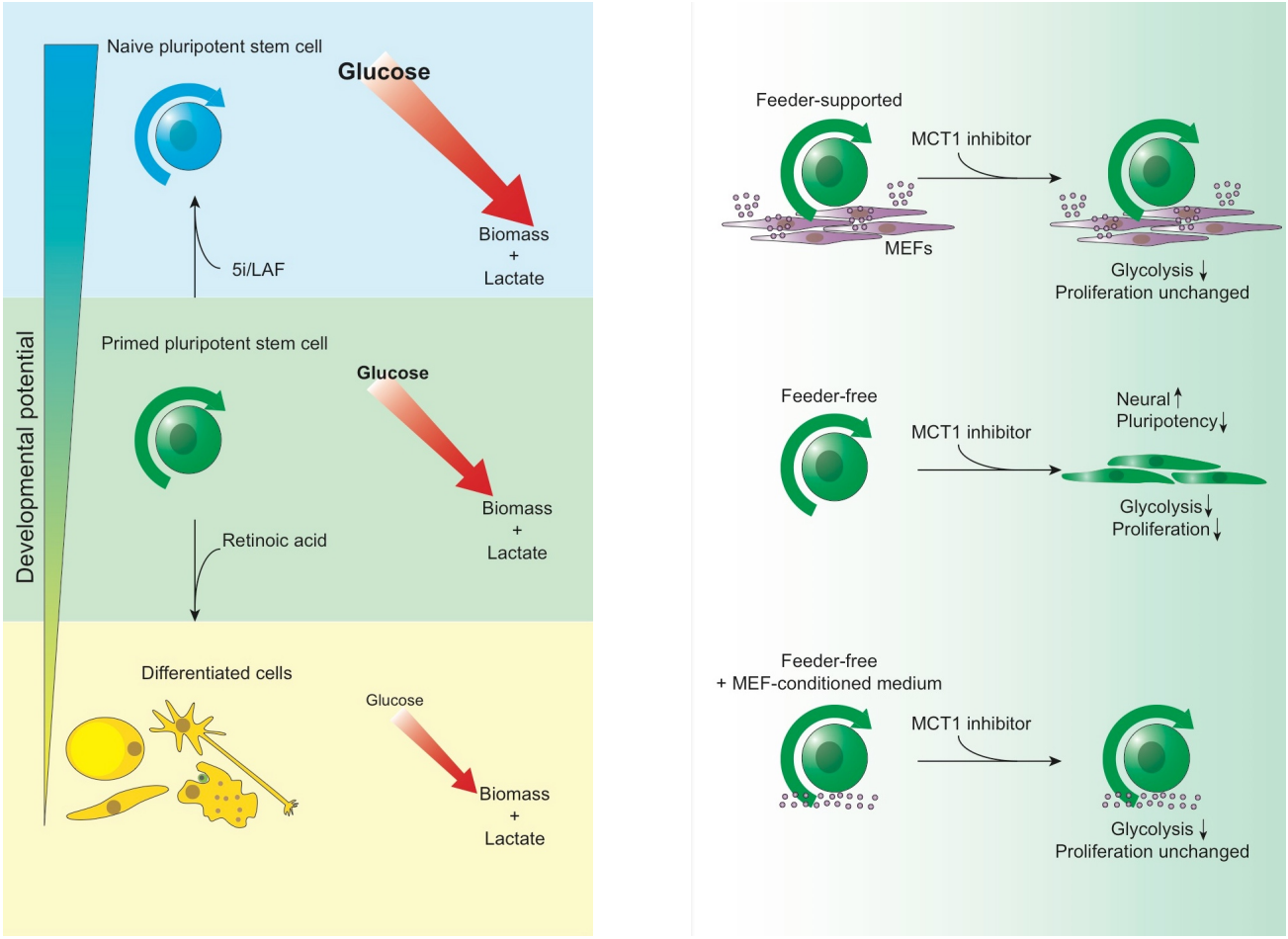

Schematic representation of the association between pluripotency and glycolytic rate, and the impact of MCT1 inhibition on primed hESC metabolism, proliferation, and differentiation.

Figure 1-25

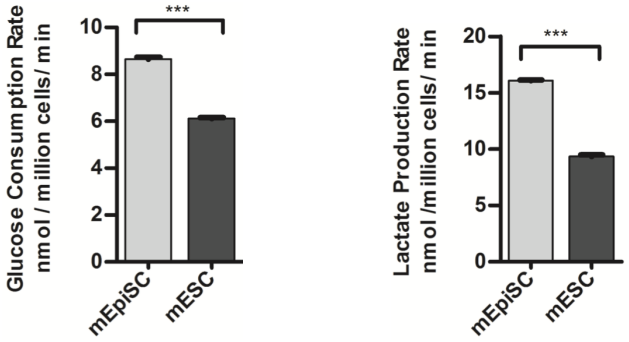

Mouse naive ESCs (mESC) exhibit lower glycolytic rates compared to mouse primed ESCs (Mouse Epiblast Stem Cells, mEpiSCs). Glucose consumption rates (left) and lactate production rates (right) of mEpiSCs derived from in vivo epiblast and mESCs cultured in 2i/LIF condition. Error bars indicate ± 1 SEM of biological replicates (n = 3). Error bars indicate ± 1 SEM of biological replicates (n = 3). *** $p < 0.001$.

Figure 1-26

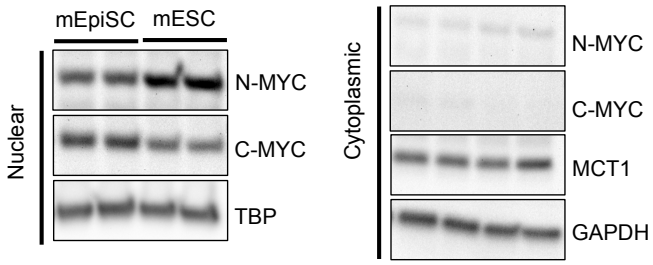

Lower nuclear C-MYC levels in mESCs versus mEpiSCs. Immunoblot showing nuclear and cytoplasmic N-MYC and C-MYC levels in mEpiSCs derived from in vivo epiblast and mESCs cultured in 2i/LIF condition. Cytoplasmic MCT1 levels are also shown. TBP is used a loading control for the nuclear lysates. GAPDH is used as a loading control for the cytoplasmic lysates. Lysates were prepared in biological duplicates.

CHAPTER 2. Manipulation of human embryonic stem cell metabolism

Introduction

Since our results support a link between MYC-driven glycolytic metabolism and the pluripotent state, we hypothesize that inhibition of glycolysis may negatively impact human pluripotency or promote differentiation. To test this hypothesis, we need to first find effective means to manipulate glycolytic metabolism in hESCs.

Genetically modifying the human pluripotent stem cells, i.e. knocking out or knocking down a certain glycolytic protein, is technically challenging. Homologous recombination (Zwaka and Thomson, 2003) and chemical transfection (Eiges et al., 2001) have both been demonstrated successfully in introducing transgenes in hESCs, yet with very low efficiency, estimating at 1 transfected cell per 10^5 hESCs. Lentiviral transduction offers a much higher efficiency at 70% (Xiong et al., 2005), and the transgenes can be integrated permanently into the host genome for stable and inheritable expression. However, in up to 95% of the lentiviral transduced hESCs, the transgenes are inactivated right after the transduction and integration process (Xia et al., 2007), likely due to epigenetic modifications of the viral DNA after its integration (Pannell et al., 2000; Yao et al., 2004). This leaves us with the option of using small molecules to target proteins involved in glycolysis.

Many glycolytic enzymes and transporters can be potentially targeted pharmaceutically to reduce glycolysis, e.g. glucose transporters (Minutolo et al., 2011), hexokinase (Penso and Beitner, 1998), glucose-6-phosphate isomerase (Meng et al., 1999), phosphofructokinase (Jeon et al., 2011), aldolase (Gefflaut et al., 1996), glyceraldehyde-3-phosphate dehydrogenase (Harris and Waters, 1976), phosphoglycerate kinase (Mcharg and Littlechild, 1996), enolase (Anderson et al., 1984), pyruvate kinase (Anastasiou et al., 2012), lactate dehydrogenase (Thornburg et al., 2008), monocarboxy transporters (Murray et al., 2005), and pyruvate dehydrogenase kinase

(Mann et al., 2000). Due to mounting evidence showing that most cancer cells have increased dependency on glycolysis (Bensinger and Christofk, 2012; Christofk et al., 2008), which is not a feature of normal cells, renewed and extensive efforts have been devoted to understanding the role of glucose metabolism in cancer, and many more glycolysis-targeting compounds are being developed or undergoing clinical trials for treating various types of tumors, which provides us a sizable pool of candidates. Many compounds of high efficacy and high specificity have been developed to target glycolysis-related proteins while minimizing off-target effects and cell toxicity. Therefore, for our purpose of studying the role of glycolysis in human pluripotency and self-renewal capacity, it is more important to find a glycolysis-related protein that is associated with pluripotent state in hESCs.

One of the proteins involved in glycolysis, Monocarboxylate Transporter 1, or MCT1, is a member of the four MCTs that catalyze proton-linked transport of monocarboxylates, such as lactate, pyruvate, and ketone bodies, across the plasma membrane (Halestrap, 2011). MCT1 facilitates both the influx and the efflux of its substrates, and the net rate of transport depends on the concentration gradients of protons and monocarboxylates on each side of the plasma membrane (Wang et al., 1994). A class of highly specific small molecule inhibitors towards MCT1 have been developed by AstraZeneca and have been applied initially for immunosuppressive therapy (Guile et al., 2006; Murray et al., 2005). Among them, AZD3965 is a potent and selective inhibitor of MCT1 with a binding affinity of 1.6 nM, which is 6-fold more selective than MCT2, with no inhibition of MCT4 at 10 μM, and has been demonstrated to decrease lactate export and inhibit cell growth in lymphoma cell lines that preferentially express MCT1 (Critchlow et al., 2012). Both having been reported to promote glycolytic flux, MCT1 is a known target regulated by the transcription factor MYC (Doherty et al., 2014), while MCT4

has been shown to be transcriptionally activated by hypoxia-inducible factor 1, or HIF-1(Denko, 2008).

Results

Manipulation of hESC metabolism via MCT1 inhibition

To identify a glycolysis-related protein that would serve as a good target for hESC metabolism manipulation, we first examined the mRNA expression levels of metabolic genes important for glycolysis towards which small molecule inhibitors have been developed. As shown in Figure 2-1, we found that Solute Carrier 16A1 (*SLC16A1*) mRNA levels significantly correlate with the pluripotent state across a panel of pluripotent cell lines and somatic cell lineages. *SLC16A1* is expressed at high levels in both primed hESCs and hiPSCs, but relatively low levels in non-pluripotent cell lines and tissues (Figure 2-1). An important target of MYC-driven glycolysis in cancer, *SLC16A1* encodes Monocarboxylate Transporter 1 (MCT1), which transports lactate, pyruvate, and other monocarboxylates across the plasma membrane in a proton-linked bidirectional manner (Adijanto and Philp, 2012; Doherty et al., 2014). An inhibitor of MCT1 activity called AZD3965 is currently undergoing Phase I evaluation for cancer treatment and reduces glycolytic rate and proliferation of cancer cell lines *in vitro* by decreasing lactate export rate (Polanski et al., 2014). To examine whether MCT1 protein level is associated with the pluripotent state, we measured MCT1 levels in lysates from primed versus naive hESCs, and in primed hESCs treated with DMSO or treated with retinoic acid for seven days to induce differentiation. MCT1 levels are modestly elevated in naive versus primed hESCs (Figure 1-20). Compared to DMSO-treated primed hESCs, MCT1 levels are markedly reduced, and OCT4A levels are absent, in retinoic acid-treated primed hESCs (Figure 2-2). Together, these results indicate that high MCT1 expression is associated with the pluripotent state and may serve as a good target for inhibition of glycolysis in hESCs.

To test whether MCT1 inhibition reduces hESC glycolytic rate, we compared the glucose consumption and lactate production rates of naive versus primed feeder-supported hESCs, and feeder-supported (FS) versus feeder-free (FF) primed hESCs treated with DMSO or AZD3965. MCT1 inhibition via AZD3965 treatment reduces glucose consumption and lactate production rates in all hESC types tested: naive feeder-supported, primed feeder-supported, and primed feeder-free hESCs (Figures 2-3 and 2-4). To our knowledge, feeder-free naive hESCs cannot be successfully derived using the 5i/LAF method. In addition, MCT1 inhibition increases oxygen consumption rate in FF hESCs (Figure 2-5). These results demonstrate that MCT1 inhibition is a feasible strategy to manipulate hESC glucose metabolism without toxic side-effects.

To determine whether reduction of glycolytic flux impacts hESC self-renewal capacity, we compared the proliferation rates of hESCs treated with DMSO versus AZD3965. Notably, we observed a proliferative impairment in naive FS hESCs, but not in primed FS hESCs (Figure 2-6). These results are consistent with our metabolomics results demonstrating increased use of glucose for biosynthesis of nucleotides and serine in naive versus primed hESCs (Figures 1-10 and 1-12). Furthermore, we found that MCT1i inhibition via AZD3965 treatment decreases proliferation rate of FF primed hESCs, but not of FS primed hESCs (Figure 2-7). Treatment with another glycolytic inhibitor, dichloroacetic acid (DCA), similarly decreases proliferation rate of FF primed hESCs, but not of FS primed hESCs (Figure 2-8). These results indicate that primed hESCs react to decreased glycolytic rate differently depending on the presence/absence of mouse embryonic fibroblasts (MEFs), and could suggest that the presence of feeder cells makes primed hESCs less reliant on glycolysis for proliferation.

MCT1 inhibition of feeder-free cultured primed hESCs promotes neural lineage specification

Since MCT1 inhibition through AZD3965 treatment reliably reduces glycolytic metabolism of FS and FF primed hESCs (Figure 2-3), we next assessed whether moderate suppression of glycolysis by MCT1 inhibition has a causal effect on the differentiation status of primed hESCs. We first noticed that five days of AZD3965 treatment causes FF hESCs to exhibit altered morphology relative to DMSO-treated hESCs. AZD3965-treated FF hESCs appear elongated, spindle-like, and more light-reflective compared to the round and smooth-edged DMSO-treated cells (Figure 2-9).

Because we had observed metabolic changes in FF primed hESCs in as little as 30 minutes post MCT1 inhibition, we first measured gene expression changes at five hours to determine whether moderate suppression of glycolysis could affect differentiation status. We sequenced the transcriptome of H9 FF hESCs at five hours post DMSO or AZD3965 treatment, and examined the gene expression differences for patterns of differentiation to particular cell types. While few genes were consistently changed at this short time point of treatment, we did find that MCT1 inhibition promoted elevated expression of the genes involved in early specification of the neural tube including ZIC5, ZIC2, EGR1, and NPTX1, and reduction of the pluripotency markers Inhibitor of Differentiation (ID1) and NANOG (Figure 2-10). Gene ontology analysis of gene expression profiling after five days of AZD3965 treatment demonstrated a clear shift in expression that appeared to correlate with neural specification (Figure 2-11 and Figure 2-12). Together with data from the five-hour time point, it seems clear that the inhibition of glycolysis with AZD3965 could, at a minimum, lower the threshold for neural specification from primed hESCs.

To assay whether MCT1 inhibition could promote neural specification under differentiation conditions, we subjected FF primed hESCs according to a well described neural specification protocol (Chambers et al., 2009). AZD3965 treatment significantly promotes the formation of neural rosette structures and neural specification compared to DMSO-treated hESCs (Figure 2-13), as judged by the increased number of SOX1 positive cells. DCA treatment does not significantly enhance neural rosette structure formation (Figure 2-14), likely due to the decreased effectiveness of 5 mM DCA treatment compared to 250 nM AZD3965 treatment in reducing glycolysis (Figures 2-3 and 2-8). Our results collectively demonstrate that glycolytic rate in human pluripotent stem cells is tightly correlated with differentiation status, from naive to primed to specified cell types.

Discussion

We have identified MCT1 as a target for inhibiting glycolysis in hESCs based on its close association with human pluripotent state, and demonstrated that AZD3965, a small molecule inhibitor towards MCT1, at 250 nM, is effective in reducing glycolytic rates in feeder-supported naive hESCs, feeder-supported primed hESCs, and feeder-free primed hESCs, without any observed cell toxicity. To our knowledge, feeder-free naive hESCs cannot be successfully maintained in 5i/LAF conditions. Therefore, in all the hESC culture systems available to us, we have demonstrated the effectiveness of AZD3965 as a glycolysis inhibitor. We have also tested other previously reported glycolysis inhibitors, such as DCA, sodium oxamate, and 3-bromopyruvate, all of which need to be used at much higher concentrations to show modest inhibitive effects on glycolysis in hESCs, often with considerable cell toxicity (data unpublished), likely due to the lack of specificities of those compounds. Interestingly, we observed a proliferative impairment by AZD3965, only in feeder-supported naive hESCs, but not in feeder-supported primed hESCs, suggesting that high glycolytic flux might be more important for the proliferation of naive hESCs than primed hESCs. Moreover, MCT1 inhibition via AZD3965 decreases the proliferation of only feeder-free primed hESCs, but not that of feeder-supported primed hESCs, suggesting that feeder-free primed hESCs might be more reliant on glycolysis for proliferation than feeder-supported primed hESCs.

While significant effort has been applied to characterize the metabolism of human pluripotent stem cells (Prigione et al., 2010; Yoshida et al., 2009; Zhang et al., 2011, 2012), our work sheds light on how to manipulate metabolism to promote a particular cell fate. This study took a clue from gene expression data at an early time point post glycolysis inhibition and focused on studying its effects on neural progenitor specification. It is entirely possible and of

great interest that metabolic manipulation might impact and regulate differentiation processes towards other lineages as well. Understanding whether and how the epigenetic state of human pluripotent stem cells is altered by inhibition of glycolysis will be of key importance to determine in future studies. Going forward, it will also be important to determine whether promotion of hESC glycolysis can improve either the efficiency or fidelity of naive human pluripotent stem cell generation. This approach could improve efforts to generate stable human naive systems, which are currently plagued by instability of self-renewal, survival, differentiation potential, and even genomic integrity.

Figures

Figure 2-1

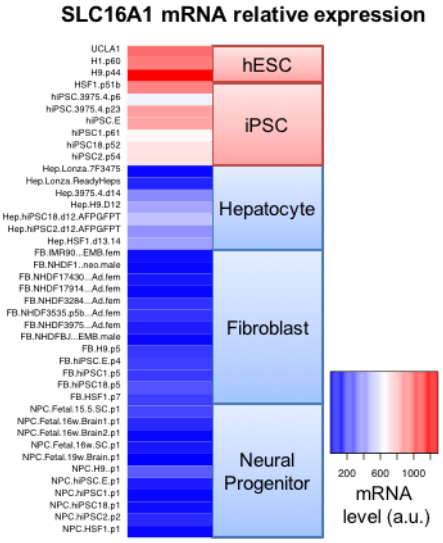

Solute Carrier 16A1 (SLC16A1) is expressed at high levels in both primed hESCs and hiPSCs, but relatively low levels in non-pluripotent cell lines and tissues. Heatmap depicting SLC16A1 mRNA levels across a panel of pluripotent and differentiated cell lines. Relative mRNA levels are color coded with a gradient from blue for the minimum through red for the maximum reading.

Figure 2-2

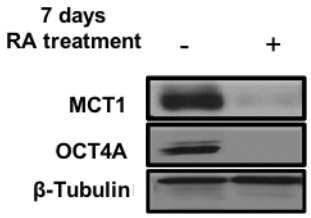

MCT1 levels are markedly reduced in retinoic acid-treated primed hESCs compared to DMSO-treated primed hESCs. Immunoblotting of lysates from H9 primed hESCs treated with DMSO or 10 μM RA treatment for 7 days and probed with antibodies towards MCT1, OCT4A, and beta-tubulin as a loading control.

Figure 2-3

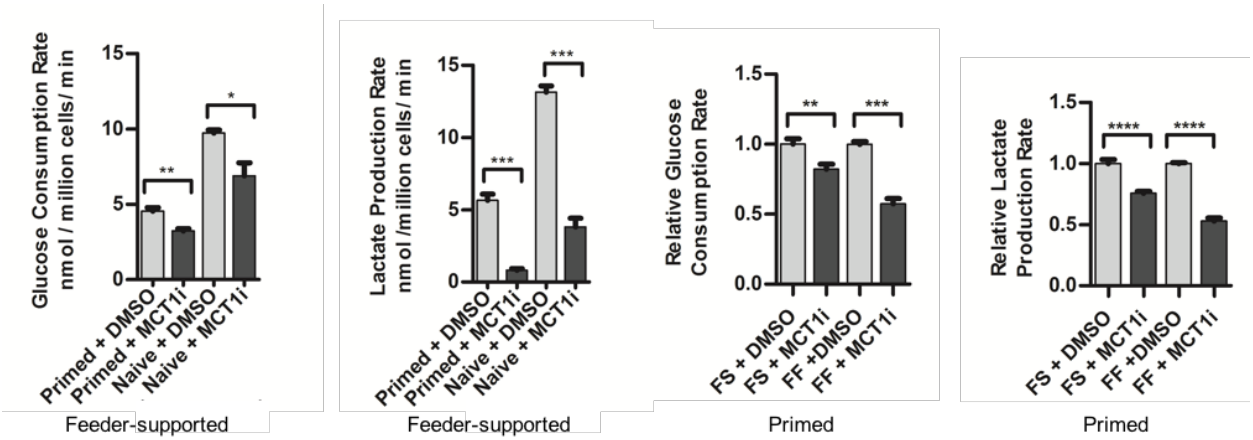

MCT1 inhibition via AZD3965 treatment reduces glucose consumption and lactate production rates in naive feeder-supported, primed feeder-supported, and primed feeder-free hESCs. Glucose consumption (left) and lactate production rates (center left) of primed versus naive feeder-supported UCLA1 hESCs treated with DMSO or 250 nM AZD3965 (MCT1i) for 24 hours. Glucose consumption (center right) and lactate production (right) rates of feeder- supported (FS) versus feeder-free (FF) cultured primed H9 hESCs treated with DMSO or 250 nM AZD3965 (MCT1i) for 24 hours. Error bars indicate ± 1 SEM of biological replicates (n = 3). * $p < 0.05$; ** $p < 0.01$; *** $p < 0.001$; **** $p < 0.0001$.

Figure 2-4

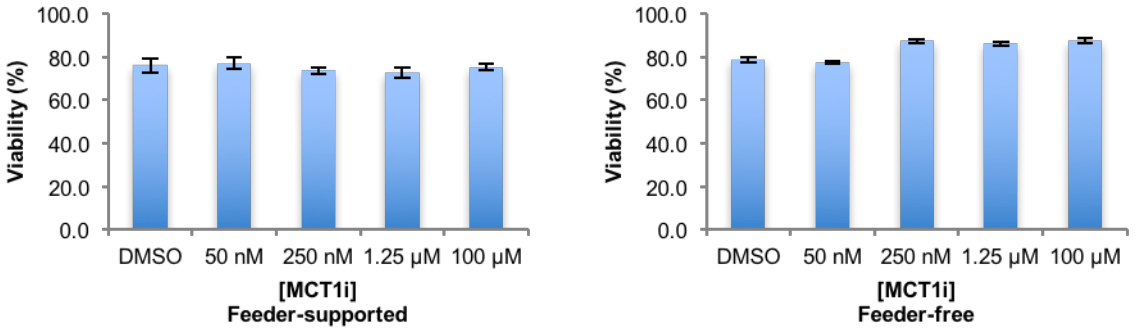

Evaluation of hESC toxicity by AZD3965. Cell viabilities of feeder-supported (A) and feeder-free (B) primed H9 hESCs treated with DMSO or AZD3965 at indicated concentrations for 24 hours, as determined by Trypan Blue staining. Error bars indicate ± 1 SEM of biological replicates (n = 3).

Figure 2-5

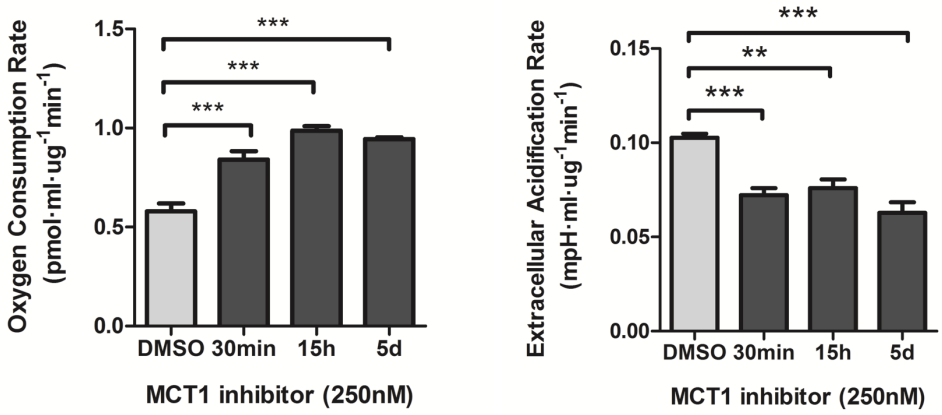

MCT1 inhibition increases oxygen consumption rate in feeder-free primed hESCs. Oxygen consumption rates (left) and extracellular acidification rates (right) in feeder-free, primed H9 hESCs, treated with DMSO or 250 nM AZD3965 for the indicated times, as measured by XF24 Extracellular Flux Analyzer. Error bars indicate ± 1 SEM of biological replicates (n = 3). ns: ** $p < 0.01$; *** $p < 0.001$.

Figure 2-6

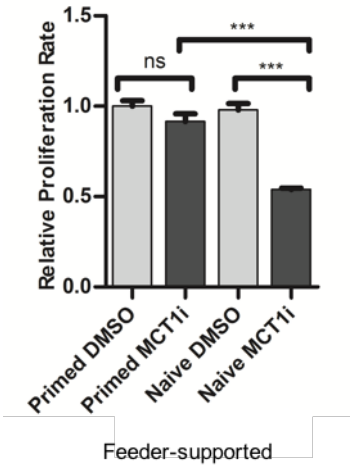

Proliferation rate is impaired in naive FS hESCs treated with AZD3965 compared to DMSO, but not in primed FS hESCs. Proliferation rates of primed versus naive feeder-supported UCLA1 hESCs treated with DMSO or AZD3965 (MCT1i) for 24 hours. Error bars indicate ± 1 SEM of biological replicates (n = 3). ns: not significant; *** $p < 0.001$.

Figure 2-7

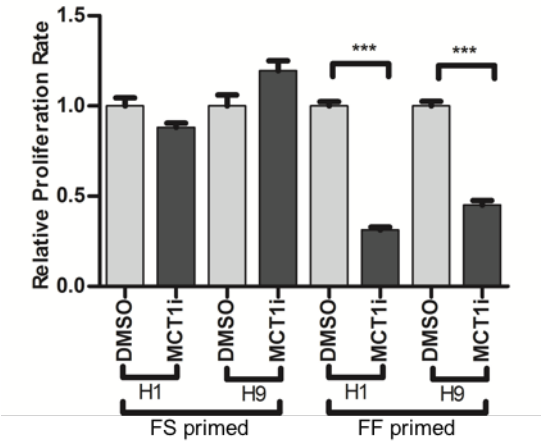

MCT1i inhibition via AZD3965 treatment decreases proliferation rate of FF primed hESCs, but not of FS primed hESCs. Proliferation rates of feeder-supported versus feeder-free H1 and H9 primed hESCs treated with DMSO or 250 nM AZD3965 (MCT1i). Error bars indicate ± 1 SEM of biological replicates (n = 3). *** $p < 0.001$.

Figure 2-8

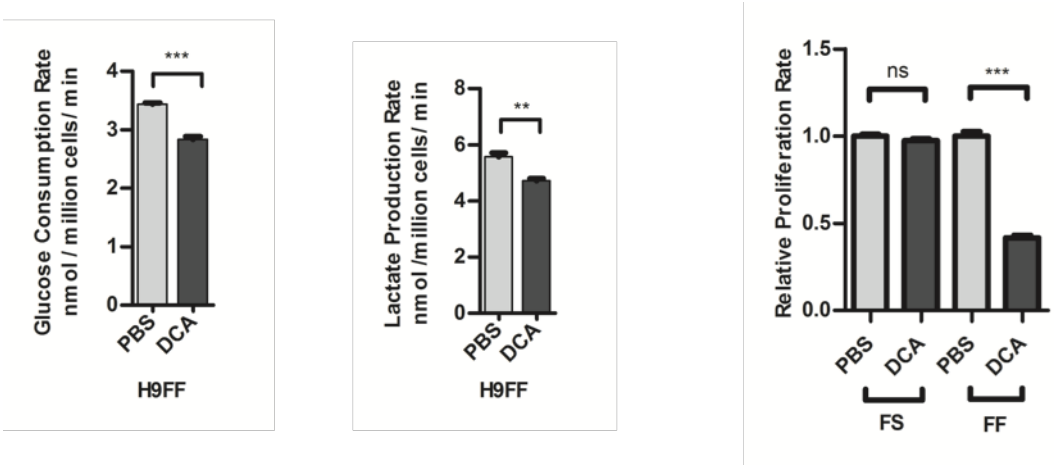

Treatment with dichloroacetic acid (DCA) reduces glycolytic rate of FF primed hESCs, and decreases proliferation rate of FF primed hESCs, but not of FS primed hESCs.

Glucose consumption rates (left) and lactate production rates (center) of FF primed H9 hESCs treated with PBS or 5 mM DCA for 24 hours. Proliferation rates (right) of feeder-supported (FS) versus feeder-free (FF) H9 hESCs treated with PBS or 5 mM DCA for 5 days. Error bars indicate ± 1 SEM of biological replicates (n = 3). ns: not significant; ** $p < 0.01$; *** $p < 0.001$.

Figure 2-9

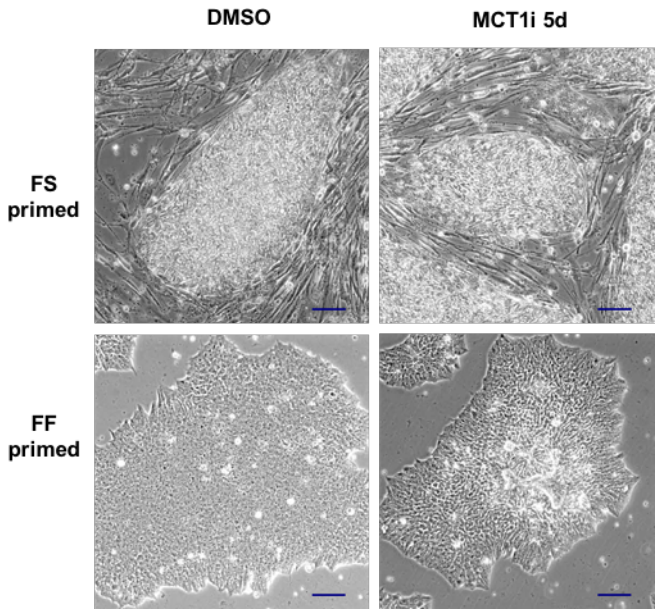

AZD3965-treated feeder-free hESCs appear elongated, spindle-like, and more light-reflective compared to the round and smooth-edged DMSO-treated cells. Phase contrast microscopic images of live FS and FF primed H9 hESCs treated with DMSO or 250nM AZD3965 (MCT1i) for 5 days (scale bar = 100 μm).

Figure 2-10

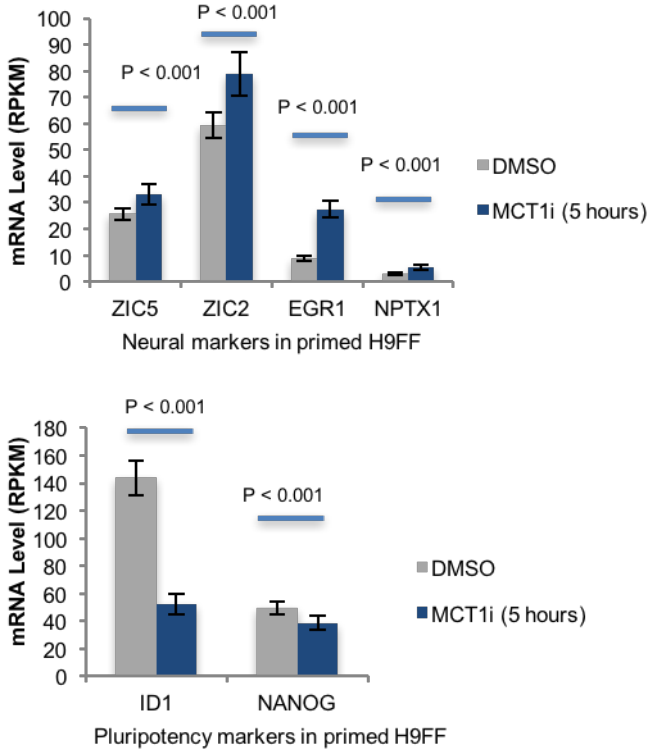

MCT1 inhibition promotes elevated expression of the genes involved in early specification of the neural tube including ZIC5, ZIC2, EGR1, and NPTX1, and reduction of the pluripotency markers Inhibitor of Differentiation (ID1) and NANOG. mRNA levels of neural markers (ZIC5, ZIC2, EGR1 and NPTX1) and pluripotency markers (ID1 and NANOG) in primed FF H9 hESCs, treated with DMSO or 250 nM AZD3965 (MCT1i) for five hours. mRNA levels were obtained by RNA sequencing biological duplicates, and expressed in RPKM (Reads Per Kilobase of transcript per Million mapped reads). Error bars indicate ± 1 SEM of biological replicates (n = 2).

Figure 2-11

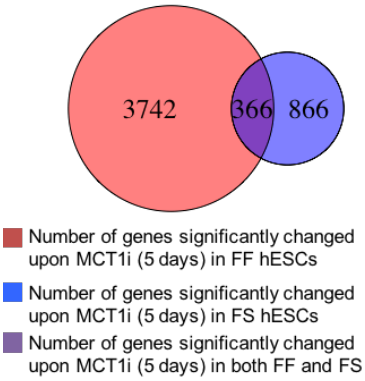

Gene Ontology Analysis on Gene Expression Changes by MCT1 Inhibition in primed FF hESCs

GO Term	Description	P-value	FDR q-value
GO:0050877	neurological system process	2.31E-11	3.13E-07
GO:0003008	system process	4.66E-11	3.16E-07
GO:0044707	single-multicellular organism process	8.68E-10	3.92E-06
GO:0032501	multicellular organismal process	1.10E-09	3.72E-06
GO:0051240	positive regulation of multicellular organismal process	1.67E-07	4.53E-04
GO:0007600	sensory perception	2.73E-07	6.16E-04
GO:0051239	regulation of multicellular organismal process	9.04E-07	1.75E-03
GO:0007186	G-protein coupled receptor signaling pathway	8.00E-06	1.35E-02
GO:0051241	negative regulation of multicellular organismal process	1.26E-05	1.89E-02
GO:0040012	regulation of locomotion	1.61E-05	2.18E-02

Gene ontology analysis of gene expression profiling after five days of AZD3965 treatment demonstrated a clear shift in expression that appeared to correlate with neural specification. Table depicting gene ontology analysis of gene expression profiling after five days AZD3965 versus DMSO treatment of primed FF H9, H1, and HSF1 hESCs.

Figure 2-12

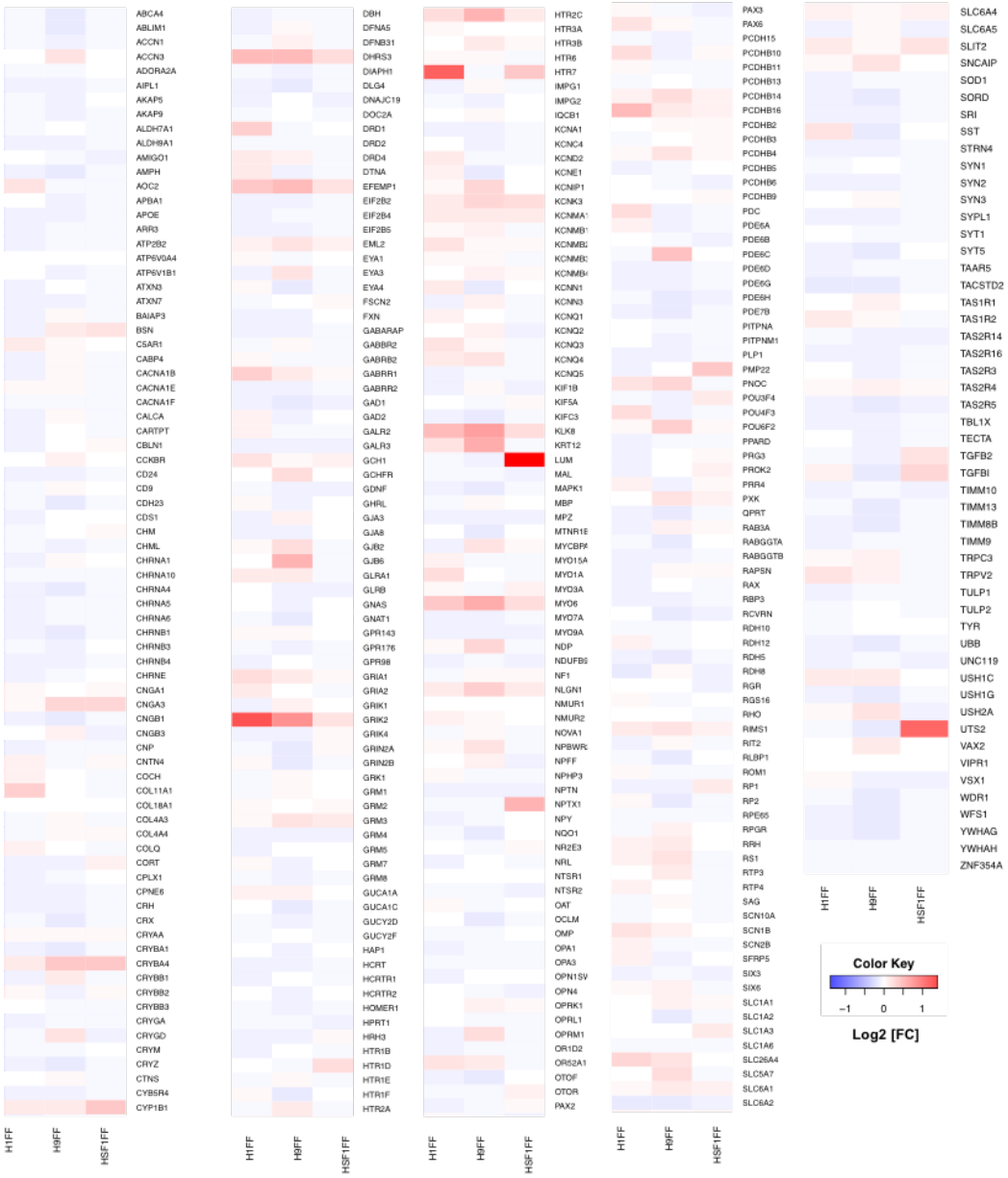

Heatmap representation of the relative fold changes (base 2) of the genes from the gene ontology term "neurological system process" after five days AZD3965 versus DMSO treatment of primed feeder-free H9, H1, and HSF1 hESCs.

Figure 2-13

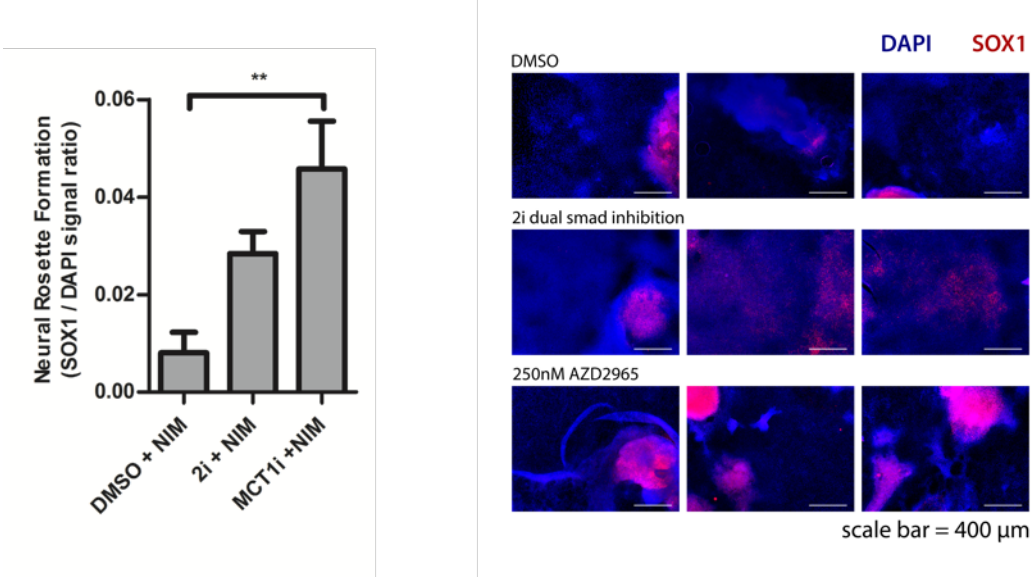

AZD3965 treatment promotes the formation of neural rosette structures and neural specification compared to DMSO-treated hESCs. Neural rosette formation efficiency of primed FF H9 hESCs treated with rosette differentiation media supplemented with DMSO, 2i dual smad inhibition (10 µM SB-431542 and 100 nM LDN193189), or 250 nM AZD3965 (MCT1i) for 10 days. SOX1 to DAPI ratio was quantified using ImageJ after acquiring immunofluorescent images from fixed cells. Corresponding images of immunofluorescence staining for SOX1 are also shown. Scale bar = 400 µm. Error bars indicate ± 1 SEM of biological replicates (n = 3). ** $p < 0.01$.

Figure 2-14

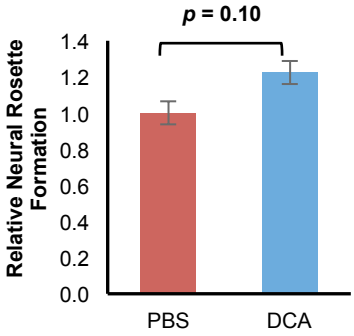

DCA treatment does not significantly enhance neural rosette structure formation. Neural rosette formation efficiency of primed feeder-free hESCs treated with rosette formation media supplemented with PBS or 5 mM dichloroacetic acid (DCA) for 10 days. The number of rosette structures was quantified. Error bars indicate ± 1 SEM of biological replicates (n = 3).

CHAPTER 3. Mouse embryonic fibroblast-secreted factors regulate primed human embryonic stem cell metabolism

Introduction

Primed hESC lines are made from blastocyst stage embryos, and were first isolated and plated into specialized media conditions that required fibroblast feeders for support (Thomson et al., 1998). However, over the past decade, development of new media compilations involving supra-physiologic amounts of fibroblast growth factor have enabled culturing of human ESCs in "feeder-free" conditions (Ludwig et al., 2006). The ability to maintain and grow hESCs and hiPSCs in feeder-free defined media has substantially improved the consistency and simplicity of both culture and differentiation (Lu et al., 2006; Peiffer et al., 2008; Rajala et al., 2010). However, a complete accounting of physiological differences of hESCs in feeder versus feeder-free culture is currently lacking.

In feeder-supported hESC culture system, the feeder layers, consisted of mouse embryonic fibroblasts, are required to maintain the pluripotent state of hESCs, and the absence of feeders leads to readily differentiation of hESCs (Consortium et al., 2010), suggesting tropic factors secreted by MEFs, and/or their role as extracellular matrix are potentially important for the maintenance of hESC pluripotency and self-renewal capacity. Since identifying the factors secreted by MEFs represents a viable strategy to understand the molecular cues and signaling pathways that are important for proliferation and pluripotency of hESCs, multiple studies have been dedicated to analyzing the protein components in the MEF-conditioned medium (Bendall et al., 2009; Buhr et al., 2007; Chin et al., 2007; Lim and Bodnar, 2002; Prowse et al., 2005, 2007; Xie et al., 2005). Depending on the detection methods used, hundreds, if not thousands, of proteins have been identified in the MEF-conditioned medium, many of which point to several pathways that may be implicated in hESC pluripotency: Wnt, BMP/ TGF-β1, activin/inhibin, and IGF-1 pathways. Notably, one of the studies, by Chin et al, took advantage of an isogenic

and non-supporting MEF line (ΔE-MEF), compared its conditioned medium with that of regular, supporting MEF-conditioned medium, and identified six proteins that are important for hESC culture: MCP-1, IL-6, PAI-1, IGFBP-2, and IGFBP-7 (Chin et al., 2007). Remarkably, when supplemented with these six proteins in unconditioned and serum-free medium, a feeder layer is not needed to support the growth of hESCs in undifferentiated state (Chin et al., 2007), suggesting that those six proteins might be responsible for the effect of MEF-conditioned medium in maintaining hESC proliferation and pluripotency.

While both feeder-supported and feeder-free culture systems appear to maintain the pluripotent state, it is critical to know what physiological differences are prevalent, especially as hESCs and hiPSCs grown in feeder-free conditions move toward clinical applications. Here we examine glucose metabolism in primed hESCs across culture systems, and the role of mouse embryonic fibroblast-secreted factors in reprogramming the hESC metabolism. By doing so, we provide key insights into the regulation of hESC metabolism, and suggest potential improvements to feeder-free conditions for hESC culture.

Results

Feeder-free-cultured primed hESCs exhibit increased anabolic glucose metabolism relative to feeder-supported primed hESCs

The differential effect of MCT1 inhibition on proliferation of FS primed hESCs versus FF primed hESCs (Figure 2-3) suggests that FS and FF hESCs use glucose differently, and that FF hESCs may use glucose more for biosynthetic pathways that support proliferation. To test this possibility, we compared the glucose consumption and lactate production rates of FS and FF primed H1 and H9 hESCs. We found H1 and H9 FF hESCs consume more glucose and produce more lactate compared to FS cells (Figure 3-1). To further determine whether FS and FF hESCs metabolize glucose differently, we labeled the cells with 1,2-^{13}C-glucose, and traced the incorporation of ^{13}C into downstream glucose metabolites using LC-MS. To control for the presence of feeder cells in the FS conditions, we also labeled a plate of irradiated MEFs without hESCs with 1,2-^{13}C-glucose, and traced the incorporation of ^{13}C into downstream glucose metabolites. Consistent with the small relative number of MEFs compared to hESCs in FS conditions (usually 2-10%), the relative amounts of metabolites as measured by LC-MS from the feeder-only plate were much smaller (0.2-10% depending on the metabolite). We determined that the presence of MEF-derived metabolites in our FS hESC metabolite samples only has a minor effect on the overall labeling pattern (Figures 3-2 and 3-3). We found that two independent primed hESC lines, H1 and H9, exhibit markedly different patterns of glucose utilization depending on whether they are cultured in FS or FF conditions (Figures 3-4 and 3-5).

The consistent metabolic changes in H1 and H9 primed hESCs in FF versus FS conditions suggest increased incorporation of glucose carbons into metabolites used for biosynthesis in FF conditions. For example, FF H1 and H9 hESCs incorporate more glucose

carbons into citrate, an important metabolic intermediate for fatty acid, cholesterol, and hexosamine biosynthesis (Figures 3-6 and 3-7). However, FF hESCs incorporate significantly less glucose carbons into other TCA metabolites than citrate, such as αKG, succinate, fumarate, and malate (Figures 3-6 and 3-7), consistent with increased use of the glucose-derived citrate for biosynthesis rather than for maintenance of TCA cycle. Additionally, FF hESCs incorporate more glucose carbons into serine and glycine, products of the serine synthesis pathway important for purine synthesis, glutathione synthesis, protein synthesis, and synthesis of lipid head groups (Rabinowitz and Vastag, 2012) (Figures 3-8 and 3-9). FF hESCs also incorporate more glucose carbons into nucleotides, including IMP, AMP, ADP, ATP, and UMP (Figures 3-10 and 3-11). These data suggest that FF primed hESCs use glucose more for biosynthesis than FS hESCs.

MEF-secreted factors make primed hESCs less reliant on glucose for proliferation

To further investigate the source of metabolic differences between FS and FF culturing methods, we assessed whether fibroblast feeder cell-secreted factors impact the response of primed hESCs to MCT1 inhibition. We incubated FF medium with irradiated MEFs in the absence of hESCs for 24 hours and collected MEF-conditioned medium. We then examined whether MEF-conditioned medium impacted the proliferation response of FF hESCs to MCT1 inhibition. As shown in Figure 3-12, MEF-conditioned medium rescues the proliferation defect caused MCT1 inhibition of FF H1 and H9 hESCs (Figure 3-12) without causing differentiation (Figure 3-13). To determine if MEF-conditioned medium rescues the proliferation defect of AZD3965-treated hESCs by restoring the glycolytic rate blunted by MCT1 inhibition, we measured glucose consumption and lactate production rates in MEF-conditioned medium treated FF cells treated with DMSO or AZD3965. We found that MEF-conditioned medium does not

alter the inhibitory effect of AZD3965 treatment of glycolysis (Figure 3-14). These data suggest that MEFs can impact hESC metabolism, at least partially by secreting factors(s) that reduce reliance of primed hESCs on glucose for proliferation.

MYC activity in primed hESCs is modulated by MEF-secreted factors

To examine the mechanism by which MEF-secreted factors reprogram primed hESC metabolism., we conducted Gene Set Enrichment Analysis (GSEA) on mRNA microarray data from FS versus FF primed hESCs, and from FF primed hESCs cultured in MEF-conditioned medium. Notably, we found that MYC-regulated gene sets are significantly enriched in FF compared to FS hESCs (Figure 3-15). Additionally, MYC-regulated gene sets are significantly enriched in FF hESCs compared to FF hESCs cultured for 24 hours in MEF-conditioned medium (Figure 3-16), suggesting that MEF-secreted factor(s) decrease MYC transcriptional activity in FF hESCs. We next examined the levels of nuclear N-MYC and C-MYC in FS, FF, and MEF-conditioned medium-treated FF hESCs. As shown in Figure 3-17, H9 and HSF1 hESCs exhibit elevated nuclear N-MYC levels in FF conditions relative to FS conditions, and MEF-conditioned medium treatment decreases nuclear N-MYC level in FF hESCs. On the other hand, neither cytoplasmic N-MYC level nor cytoplasmic/nuclear C-MYC level is consistently altered in FS, FF, and MEF-conditioned medium-treated H9 and HSF1 hESCs (Figure 3-17). These data suggest that N-MYC may be responsible for the difference in glucose metabolism between FS and FF primed hESCs, and that N-MYC levels and transcriptional activity can be down-regulated by MEF-secreted factors.

Discussion

We have shown that feeder-free primed hESCs exhibit elevated anabolic glucose metabolism and increased reliance on glucose for proliferation. Compared to feeder-supported primed hESCs, feeder-free primed hESCs are more glycolytic, exhibit markedly different patterns of glucose utilization, and incorporate more glucose carbons into intermediates that are important for biosynthesis of fatty acid, nucleotides etc. In consistent with the idea that feeder-free primed hESCs are more reliant on glycolysis for anabolism than feeder-supported cells, glycolysis inhibition causes a dramatic proliferative impairment in feeder-free cells, while leaving the proliferation of feeder-supported cells unchanged. These data clearly point to an important role for MEF feeder cells, either due to their physical interactions with hESCs, or their secreted factors, or both, in impacting or rewiring glucose metabolism in hESCs.

We have further demonstrated that MEF-secreted factors are, at the least, partially responsible for modulating hESC metabolism and making primed hESCs less reliant on glycolysis for their proliferation. We have shown that the MEF-conditioned medium that rescues proliferation does not consistently rescue net glucose uptake or lactate production of MCT1 inhibited feeder-free primed hESCs, suggesting the rescue effect by MEF-conditioned medium is not due to a simple reversal of glycolysis inhibition, but rather because of reducing glycolysis reliance of feeder-free primed hESCs for proliferation. Of note, when we fractionate the MEF-conditioned medium by molecular weight, the fraction that rescues the proliferation is above 10 kDa, while the below 10 kDa fraction, which contains most metabolites in the conditioned medium, has no rescue effect, indicating that factors of higher molecular weight, such as proteins, are responsible for the rescue effect (Figure 3-18). Therefore, our data suggest that MEF-secreted protein factor(s) decrease primed hESC reliance on glucose for proliferation.

To identify the protein factor(s) in MEF conditioned medium that are responsible for the metabolic reprogramming effects, we collected E8 feeder-free culture medium incubated with MEFs for 24 hr, along with blank E8 medium, and E8 medium incubated with feeder-free primed hESCs for 24 hr. And then we separated the proteins within the medium samples by electrophoresis, visualized the protein bands by Coomassie staining, and finally cut out a few bands that are specifically present in MEF-conditioned medium for protein identification by LC/MS/MS. Notably, we identified many proteins that are at high levels in MEF conditioned medium, and at much lower levels in blank medium or FF hESC-conditioned medium: plasminogen activator inhibitor 1 (PAI1), SPARC, Inhibin beta A chain (INHBA), Follistatin-related protein 1 (FSTL1), Collagen alpha-1(I) chain (CO1A1), Phosphoglycerate kinase 1 (PGK1), Cathepsin B (CATB), Serpin H1 (SERPH), Calumenin, Collagen alpha-2(I) chain (CO1A2), Vimentin (VIME), Pigment epithelium-derived factor (PEDF), Cathepsin D (CATD), Glia-derived nexin (GDN), Isoform 2 of Gelsolin, Elongation factor 1-gamma (EF1G), Sphingosine-1-phosphate phosphatase 1, Prelamin-A/C (LMNA), Filamin, Actin-related protein 3 (ARP3), Serpin B6 (SPB6), Proliferation-associated protein 2G4 (PA2G4), Ribonuclease inhibitor (RINI), Thioredoxin domain-containing protein 5, Platelet-derived growth factor receptor-like protein (PGFRL), Isoform 2 of Tropomyosin beta chain (TPM2), Cathepsin L1 (CATL1), Collagen alpha-1(V) chain (CO5A1), Biglycan (PGS1), Annexin A2 (ANXA2), Out at first protein homolog (OAF), Peptidyl-prolyl cis-trans isomerase D (PPID), Protein disulfide-isomerase A3 (PDIA3), Protein disulfide-isomerase (PDIA1), Protein disulfide-isomerase A6 (PDIA6), Pyruvate kinase PKM (KPYM), Carboxypeptidase E (CBPE), Calreticulin (CALR), Procollagen C-endopeptidase enhancer 1 (PCOC1). Interestingly, PAI1 was previously implicated in maintaining the growth and undifferentiated state of hESCs (Chin et al., 2007).

However, our preliminary data suggested that PAI1 alone could not rescue the proliferative defect caused by MCT1 inhibition in feeder-free primed hESCs, suggesting that other MEF-secreted factor(s) may also be responsible for the different glucose metabolic phenotype in between feeder-supported and feeder-free primed hESCs.

Relative to feeder-supported primed hESCs, we show that feeder-free primed hESCs exhibit higher MYC transcriptional activity and nuclear N-MYC levels, both of which are reduced in the presence of MEF-secreted factor(s). These results suggest that N-MYC may promote increased anabolic glucose metabolism in FF versus FS cultured primed hESCs, and that N-MYC is subject to regulation by MEF-secreted factor(s). In Chapter 1, we show that feeder-supported naive hESCs exhibit elevated glycolytic rate, higher MYC transcriptional activity, and increased nuclear N-MYC levels compared to feeder-supported primed hESCs, suggesting that hESCs with a higher degree of pluripotency are more glycolytic and their increased glycolysis might be regulated by N-MYC. However, we do not suggest the reverse is necessarily true, i.e. we do not think more glycolytic hESCs are necessarily more pluripotent. This notion is important when discuss the metabolic differences between FS and FF primed hESCs. Despite their higher glycolytic rates and increased nuclear N-MYC levels, there is no evidence suggesting that FF primed hESCs are more pluripotent than FS primed hESCs. In fact, we postulate that FS primed hESCs consume less glucose mainly because they are less reliant on glucose for anabolic metabolism.

Figures

Figure 3-1

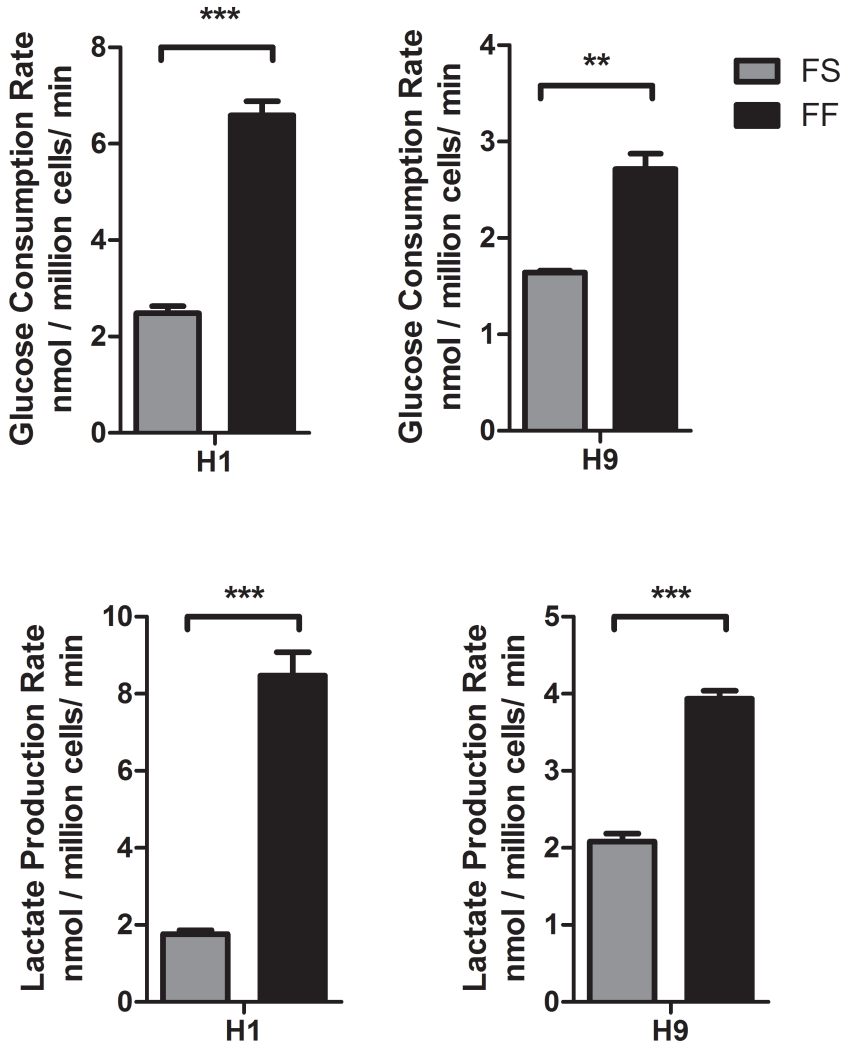

Feeder-free hESCs consume more glucose and produce more lactate compared to feeder-supported cells. Glucose consumption (top) and lactate production (bottom) rates of feeder-supported (FS) versus feeder-free cultured (FF) primed H1 (left) and H9 (right) hESCs. Error bars indicate ± 1 SEM of biological replicates (n = 3). ** $p < 0.01$; *** $p < 0.001$.

Figure 3-2

$$\text{Percent labeled} = \frac{\text{Labeled signal}}{\text{Labeled signal} + \text{Unlabeled signal}} = \frac{M_{+1} + M_{+2} + M_{+3} + \ldots + M_{+N}}{M_0 + M_{+1} + M_{+2} + M_{+3} + \ldots + M_{+N}}$$

where M_0 is the amount of the monoisotopic compound, M_{+1} is the amount of the compound with one ^{13}C atom, M_{+2} is the amount of the compound with 2 x ^{13}C atoms and so on; N is the number of carbon atoms in the molecule. (Yuan et al., 2008; Fan et al., 2014)

$$\text{Percent labeled after correction} = \frac{(\text{Labeled signal})_{\text{FS hESCs}} - (\text{Labeled signal})_{\text{MEFs}}}{[(\text{Labeled signal})_{\text{FS hESCs}} - (\text{Labeled signal})_{\text{MEFs}}] + [(\text{Unlabeled signal})_{\text{FS hESCs}} - (\text{Unlabeled signal})_{\text{MEFs}}]}$$

The formulas applied to calculate the effect of MEFs on the ^{13}C glucose labeling pattern of feeder supported hESCs.

Figure 3-3

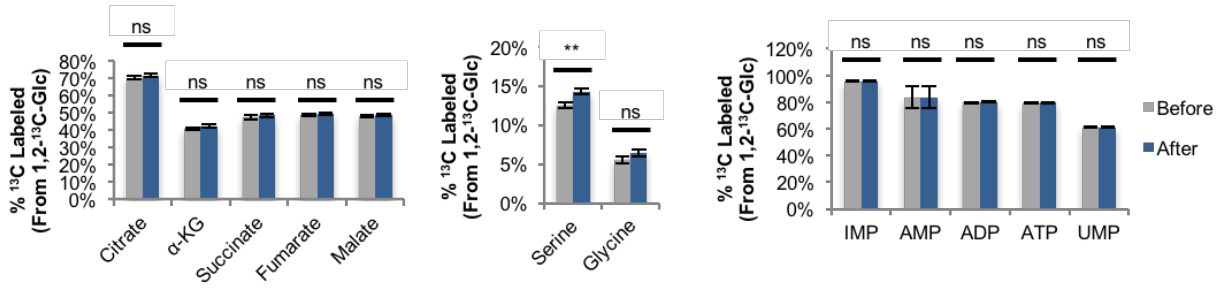

The presence of MEF-derived metabolites in our feeder-supported hESC metabolite samples only has a minor effect on the overall labeling pattern. Incorporation of ^{13}C labeled glucose into TCA cycle metabolites (left), and serine and glycine (center), and nucleotides (right) in feeder supported UCLA1 hESCs before and after the mathematical correction. Feeder supported UCLA1 hESCs and MEFs alone were cultured in medium with 1,2-^{13}C-glucose for 24 hours. Extracted metabolites were analyzed by LC-MS, and the percentage of ^{13}C-labeled metabolites was compared. Error bars indicate ± 1 SEM of biological replicates (n = 3). ns: not significant; ** $p < 0.01$.

Figure 3-4

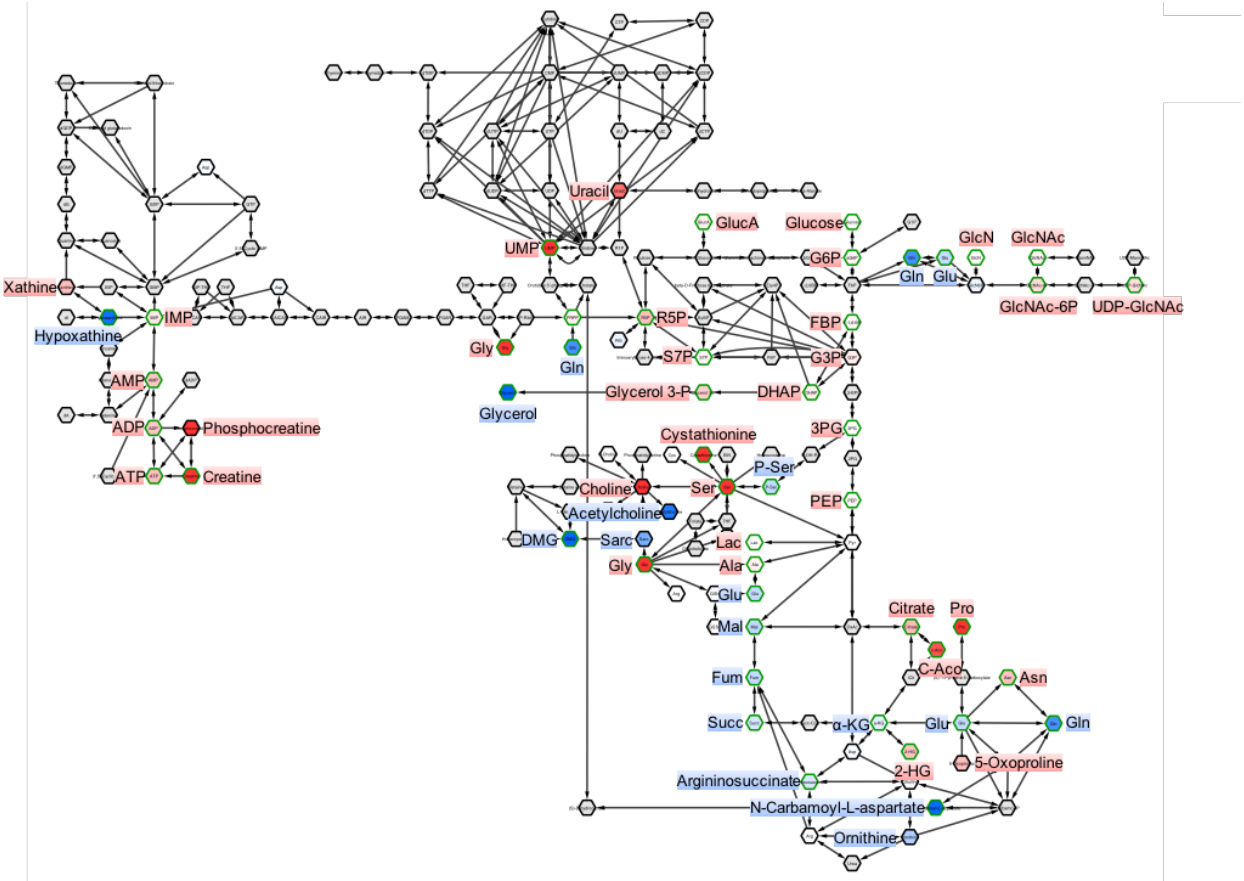

(legend on next page)

Primed H9 hESCs exhibit markedly different patterns of glucose utilization depending on whether they are cultured in feeder-supported or feeder-free conditions. Cytoscape network map showing the ratio of labeled metabolites from ^{13}C glucose in FS versus FF primed H9 hESCs. FS and FF primed H9 hESCs were cultured in medium with 1,2- ^{13}C-glucose for 24 hours. Metabolites were extracted and analyzed by LC-MS, and the percentage of ^{13}C-labeled metabolites in FS vs FF primed H9 hESCs was compared. Metabolites in red indicate increased ^{13}C-labeled metabolic pool sizes in FF hESCs compared to FS hESCs, while metabolites in blue indicate increased ^{13}C-labeled metabolic pool sizes in FS hESCs compared to FF hESCs. Green borders indicate statistically significant ($p < 0.05$) changes in incorporation of ^{13}C from 1,2-^{13}C-glucose in FS hESCs versus FF hESCs. Metabolites in white indicate similar incorporation of ^{13}C from 1,2-^{13}C-glucose in FS hESCs and FF hESCs. Metabolites in grey were undetected.

Figure 3-5

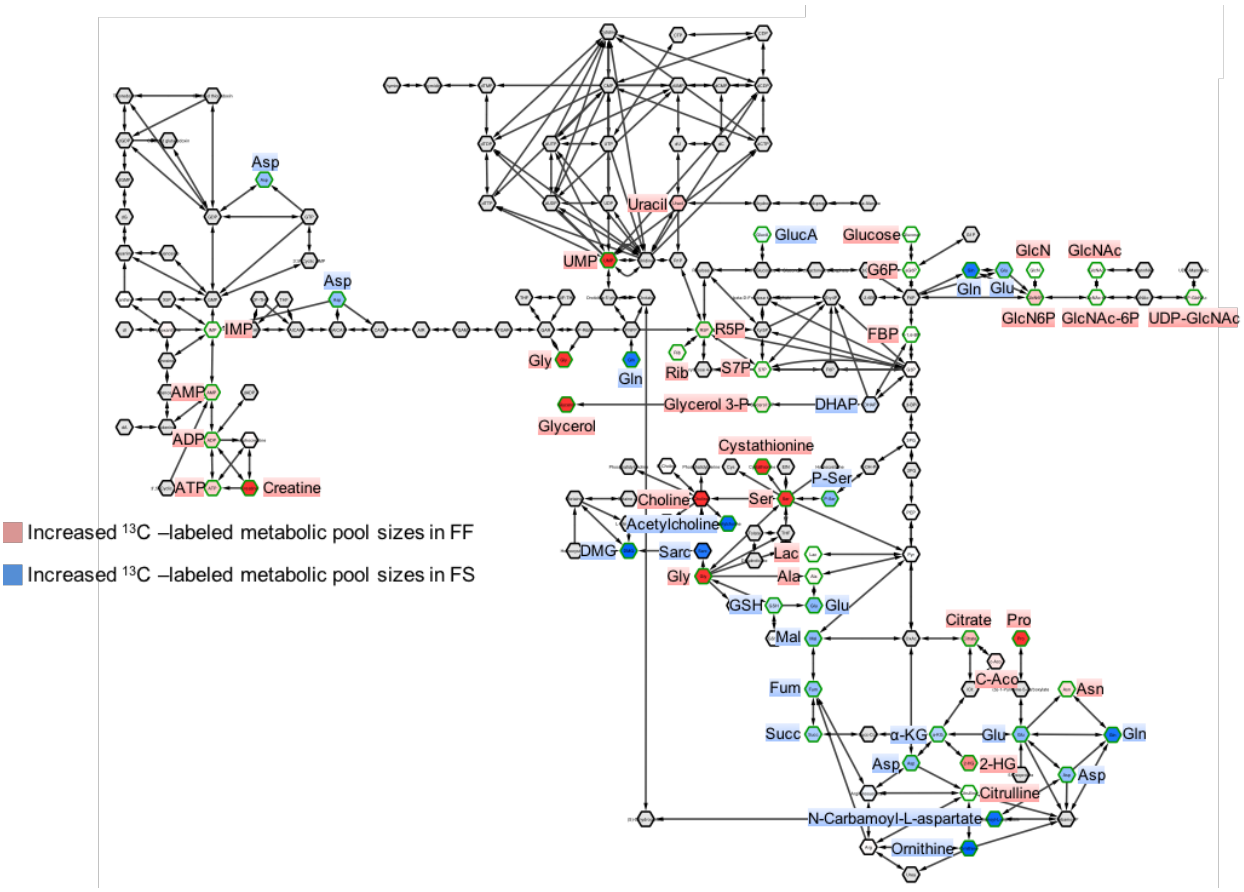

(legend on next page)

Primed H1 hESCs exhibit markedly different patterns of glucose utilization depending on whether they are cultured in feeder-supported or feeder-free conditions. Cytoscape network map showing the ratio of labeled metabolites from ^{13}C glucose in FS versus FF primed H1 hESCs. FS and FF primed H1 hESCs were cultured in medium with 1,2- ^{13}C-glucose for 24 hours. Metabolites were extracted and analyzed by LC-MS, and the percentage of ^{13}C-labeled metabolites in FS vs FF primed H1 hESCs was compared. Metabolites in red indicate increased ^{13}C-labeled metabolic pool sizes in FF hESCs compared to FS hESCs, while metabolites in blue indicate increased ^{13}C-labeled metabolic pool sizes in FS hESCs compared to FF hESCs. Green borders indicate statistically significant ($p < 0.05$) changes in incorporation of ^{13}C from 1,2-^{13}C-glucose in FS hESCs versus FF hESCs. Metabolites in white indicate similar incorporation of ^{13}C from 1,2-^{13}C-glucose in FS hESCs and FF hESCs. Metabolites in grey were undetected.

Figure 3-6

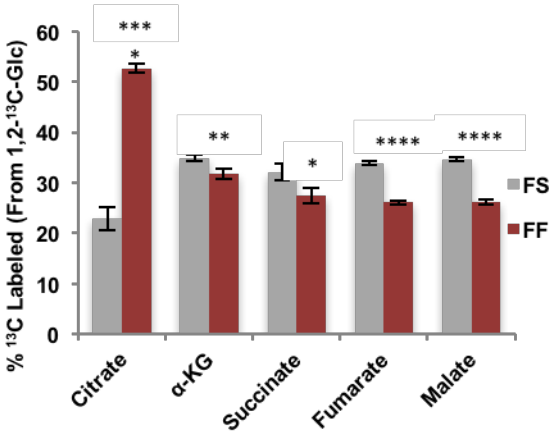

Feeder-free H9 hESCs incorporate more glucose carbons into citrate. Percentages of the indicated ^{13}C-labeled TCA cycle metabolites in FS versus FF primed H9 hESCs. FS and FF primed H9 hESCs were cultured in medium with 1,2- ^{13}C-glucose for 24 hours. Metabolites were extracted and analyzed by LC-MS, and the percentage of ^{13}C-labeled metabolites in FS vs FF primed H9 hESCs was compared. Error bars indicate ± 1 SEM of biological replicates (n = 3). * $p < 0.05$; ** $p < 0.01$; *** $p < 0.001$; **** $p < 0.0001$.

Figure 3-7

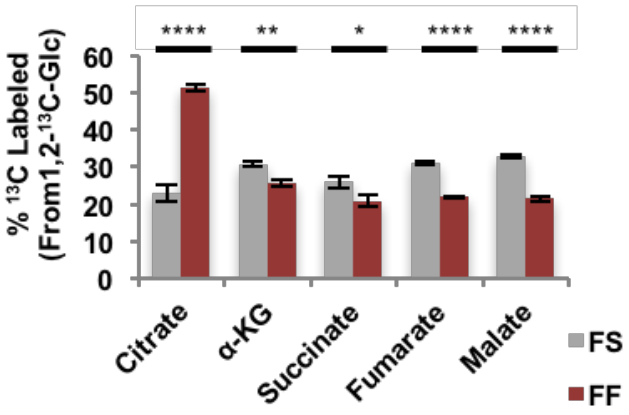

Feeder-free H1 hESCs incorporate more glucose carbons into citrate. Percentages of the indicated ^{13}C-labeled TCA cycle metabolites in FS versus FF primed H1 hESCs. FS and FF primed H1 hESCs were cultured in medium with 1,2- ^{13}C-glucose for 24 hours. Metabolites were extracted and analyzed by LC-MS, and the percentage of ^{13}C-labeled metabolites in FS vs FF primed H1 hESCs was compared. Error bars indicate ± 1 SEM of biological replicates (n = 3). * $p < 0.05$; ** $p < 0.01$; **** $p < 0.0001$.

Figure 3-8

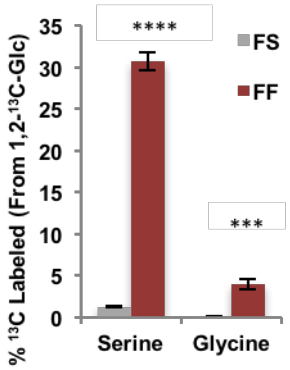

Feeder-free H9 hESCs incorporate more glucose carbons into serine and glycine compared to feeder-supported cells. Percentages of ^{13}C- labeled serine and glycine in FS versus FF primed H9 hESCs. FS and FF primed H9 hESCs were cultured in medium with 1,2- ^{13}C-glucose for 24 hours. Metabolites were extracted and analyzed by LC-MS, and the percentage of ^{13}C-labeled metabolites in FS vs FF primed H9 hESCs was compared. Error bars indicate ± 1 SEM of biological replicates (n = 3). *** $p < 0.001$; **** $p < 0.0001$.

Figure 3-9

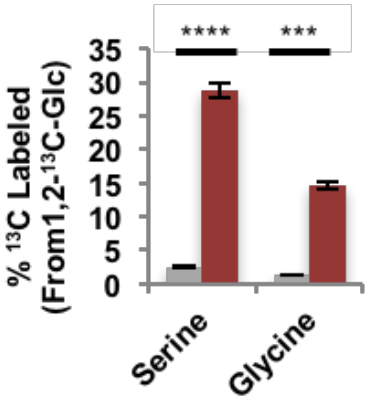

Feeder-free H1 hESCs incorporate more glucose carbons into serine and glycine compared to feeder-supported cells. Percentages of ^{13}C- labeled serine and glycine in FS versus FF primed H1 hESCs. FS and FF primed H1 hESCs were cultured in medium with 1,2- ^{13}C-glucose for 24 hours. Metabolites were extracted and analyzed by LC-MS, and the percentage of ^{13}C-labeled metabolites in FS vs FF primed H1 hESCs was compared. Error bars indicate ± 1 SEM of biological replicates (n = 3). *** $p < 0.001$; **** $p < 0.0001$.

Figure 3-10

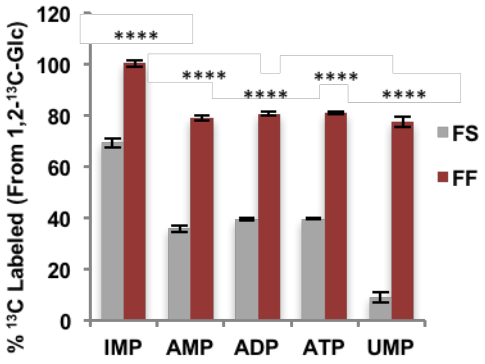

Feeder-free H9 hESCs incorporate more glucose carbons into nucleotides. Percentages of ^{13}C-labeled nucleotides in FS versus FF primed H9 hESCs. FS and FF primed H9 hESCs were cultured in medium with 1,2- ^{13}C-glucose for 24 hours. Metabolites were extracted and analyzed by LC-MS, and the percentage of ^{13}C-labeled metabolites in FS vs FF primed H9 hESCs was compared. Error bars indicate ± 1 SEM of biological replicates (n = 3). **** $p < 0.0001$.

Figure 3-11

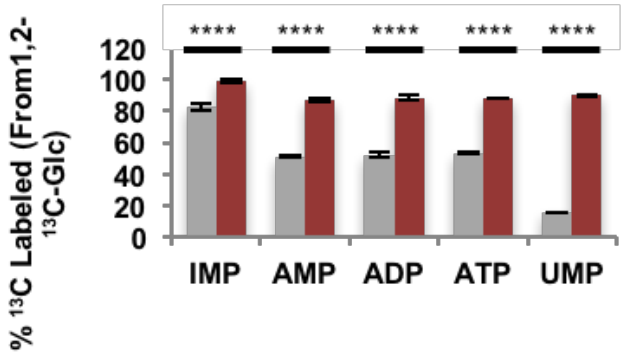

Feeder-free H1 hESCs incorporate more glucose carbons into nucleotides. Percentages of ^{13}C-labeled nucleotides in FS versus FF primed H1 hESCs. FS and FF primed H1 hESCs were cultured in medium with 1,2- ^{13}C-glucose for 24 hours. Metabolites were extracted and analyzed by LC-MS, and the percentage of ^{13}C-labeled metabolites in FS vs FF primed H1 hESCs was compared. Error bars indicate ± 1 SEM of biological replicates (n = 3). **** $p < 0.0001$.

Figure 3-12

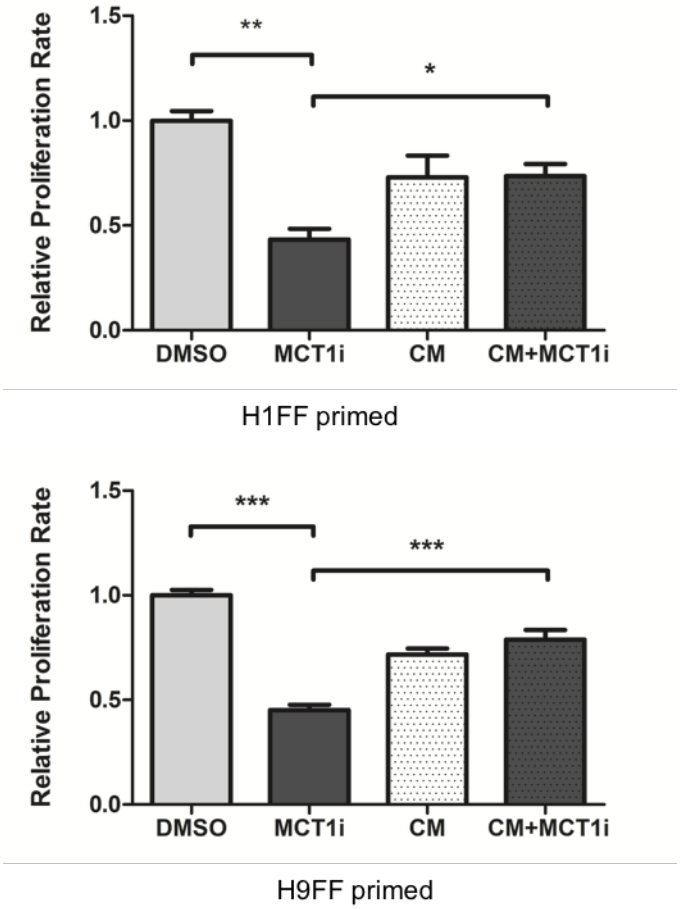

MEF-conditioned medium rescues the proliferation defect caused MCT1 inhibition of feeder-free hESCs. Proliferation rates of primed feeder-free H1 (top) and H9 (bottom) hESCs treated with DMSO, AZD3965 (MCT1i), MEF-conditioned medium (CM), or AZD3965 along with MEF- conditioned medium (CM + MCT1i) for 5 days. Error bars indicate ± 1 SEM of biological replicates (n = 3). * $p < 0.05$; ** $p < 0.01$; *** $p < 0.001$;.

Figure 3-13

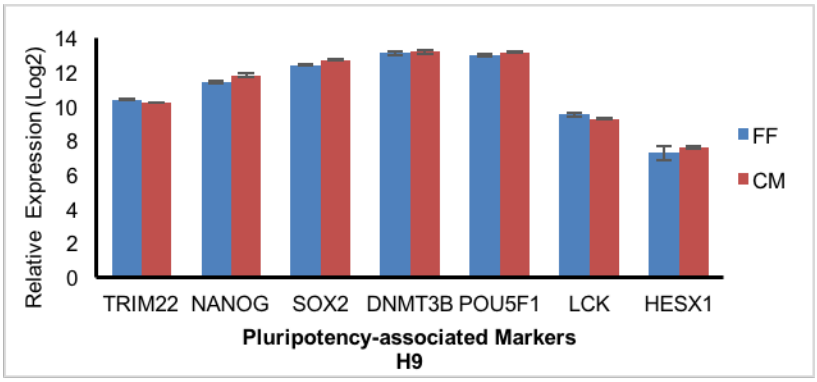

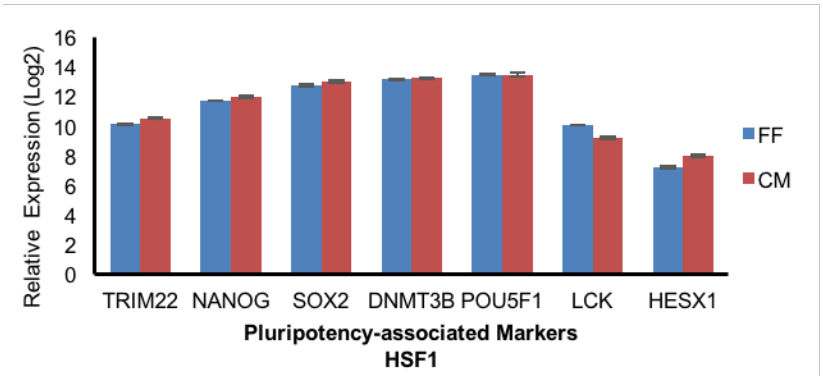

MEF-conditioned medium treatment does not change pluripotency-associated transcripts in primed feeder-free hESCs. mRNA levels of TRIM22, NANOG, SOX2, DNMT3B, POU5F1, LCK, and HESX1 in feeder- free (FF) versus MEF-conditioned medium treated FF (CM) H9 (top) and HSF1 (bottom) primed hESCs. Error bars indicate ± 1 SD of biological replicates (n=3).

Figure 3-14

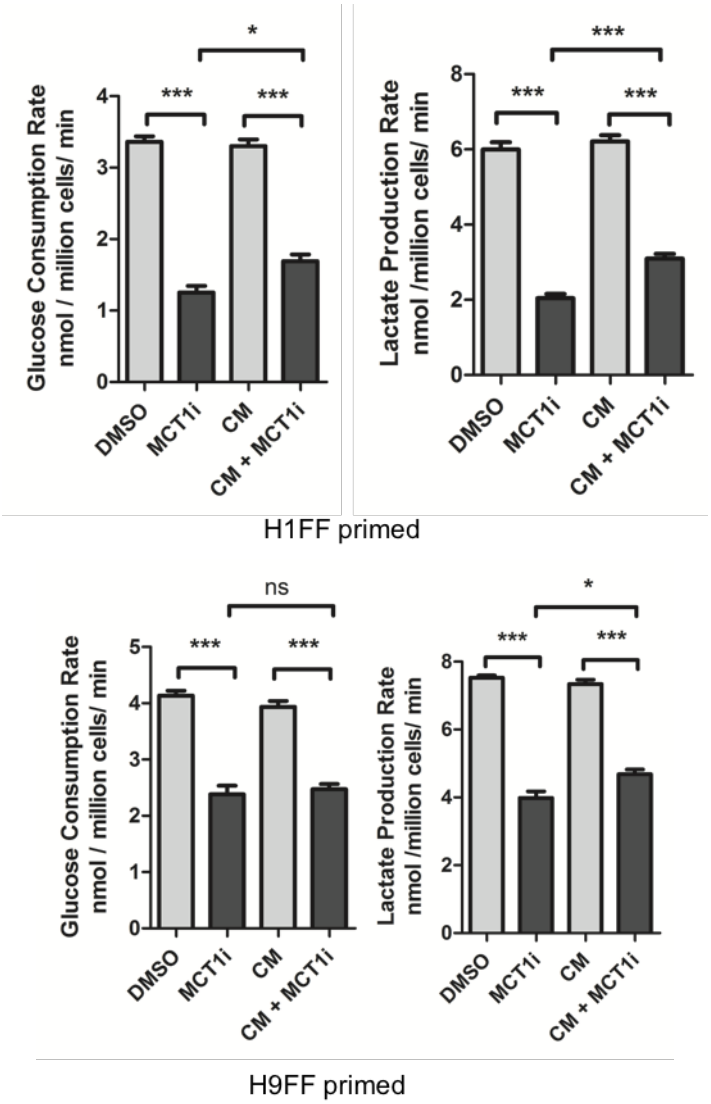

MEF-conditioned medium does not alter the inhibitory effect of AZD3965 treatment of glycolysis. Glucose consumption and lactate production rates of feeder-free H1 (top) and H9 (bottom) primed hESCs FF, treated with DMSO, AZD3965 (MCT1i), MEF conditioned medium (CM), or AZD3965 along with MEF conditioned medium (CM + MCT1i) for 5 days. Error bars indicate ± 1 SEM of biological replicates (n = 3). ns: not significant; * $p < 0.05$; *** $p < 0.001$.

Figure 3-15

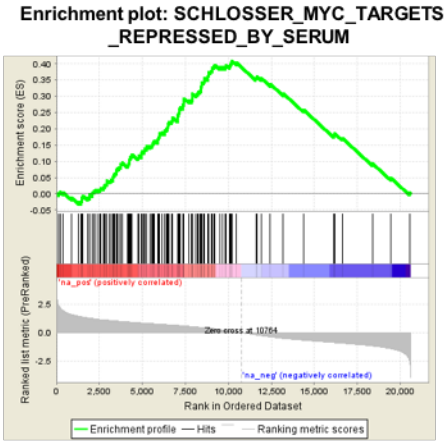

FF versus FS in primed H1, H9, and HSF1
ES = 0.41, NES = 5.41
p < 0.001, FDR < 0.001

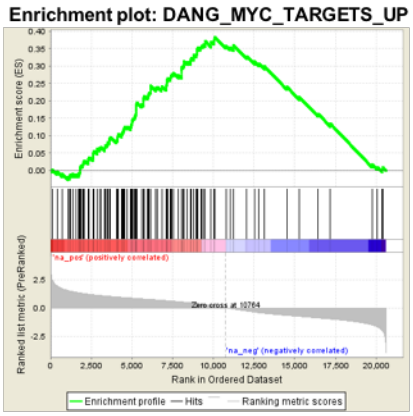

FF versus FS in primed H1, H9, and HSF1
ES = 0.38, NES = 5.06
p < 0.001, FDR < 0.001

MYC-regulated gene sets are significantly enriched in feeder-free compared to feeder-supported hESCs. GSEA mountain plots displaying enrichment of MYC-regulated gene sets in feeder-free (FF) versus feeder-supported (FS) primed H1, H9, and HSF1 hESCs.

Figure 3-16

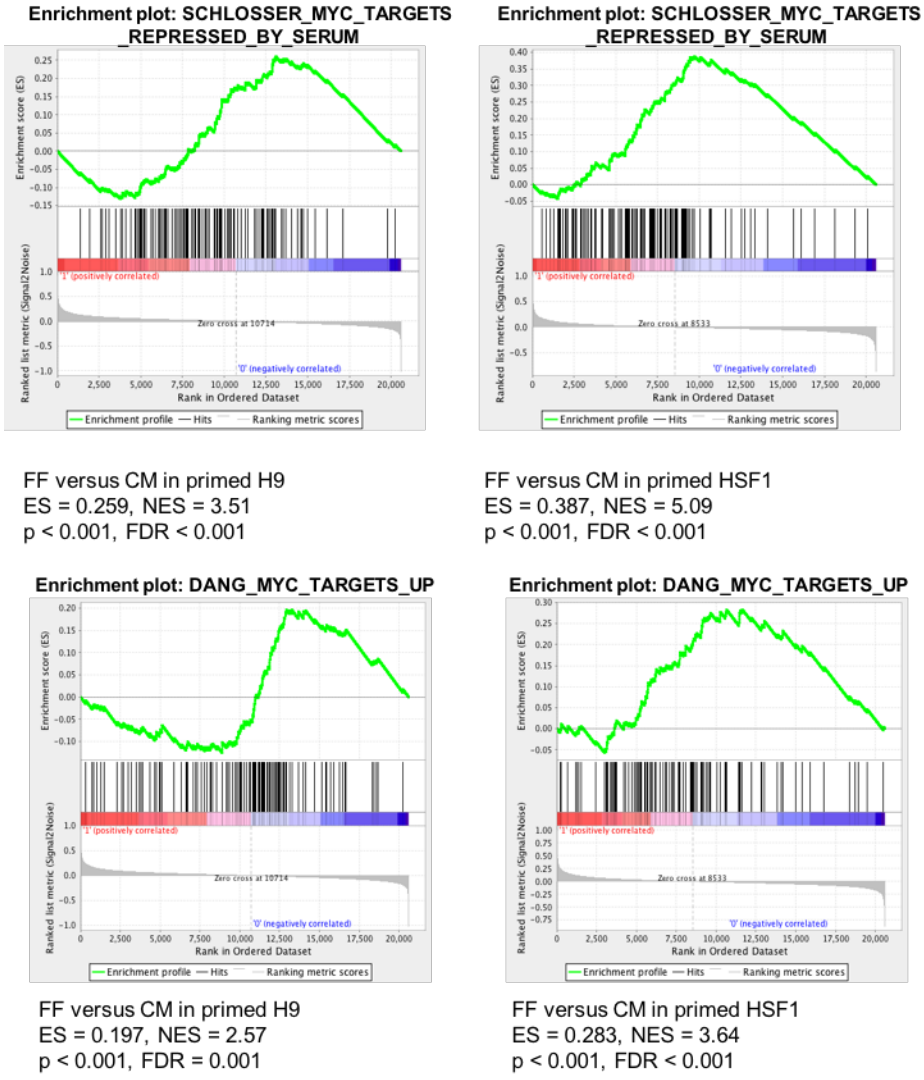

MYC-regulated gene sets are significantly enriched in feeder-free hESCs compared to feeder-free hESCs cultured for 24 hours in MEF-conditioned medium. GSEA mountain plots displaying enrichment of MYC-regulated gene sets in feeder-free (FF) versus MEF-conditioned medium treated FF (CM) primed H9 (left) and HSF1 (right) hESCs.

Figure 3-17

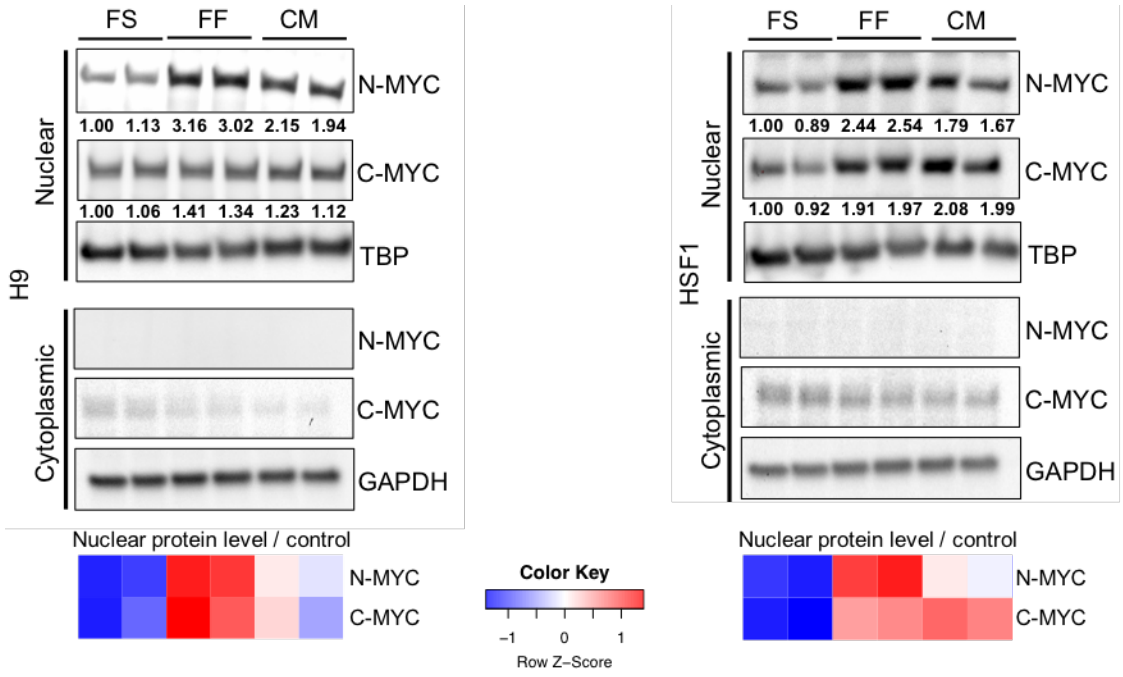

hESCs exhibit elevated nuclear N-MYC levels in feeder-free conditions relative to feeder-supported conditions, and MEF-conditioned medium treatment decreases nuclear N-MYC level in feeder-free hESCs. Immunoblot showing nuclear and cytoplasmic N- MYC and C-MYC levels in FS, FF and MEF-conditioned medium (CM) treated primed H9 hESCs (left) and HSF1 hESCs (right). The heatmap shows standardized levels of indicated markers across samples (Z score). TBP was used to control for nuclear lysate loading, and GAPDH was used to control for cytoplasmic lysate loading. Lysates were prepared in biological duplicates.

Figure 3-18

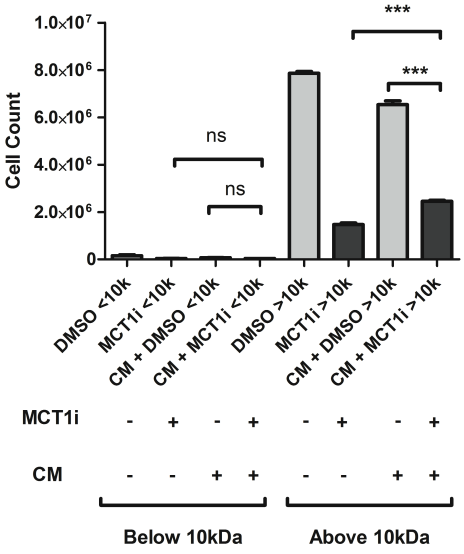

The above-10kDa fraction in MEF-conditioned medium seems responsible for its rescuing effect on the proliferative defect caused by MCT1 inhibition in primed feeder-free hESCs. Proliferation rates of feeder-free H9 hESCs in 10 kDa filtrate (i.e., material of molecular weight < 10 kDa) treated with DMSO (DMSO <10k), AZD3965 (MCT1i <10k), MEF-conditioned medium (CM + DMSO <10k), or AZD3965 along with MEF-conditioned medium (CM + MCT1i <10k) for 5 days, and in 10 kDa retentate (i.e., material of molecular weight > 10 kDa) treated with DMSO (DMSO >10k), AZD3965 (MCT1i >10k), MEF-conditioned medium (CM + DMSO >10k), or AZD3965 along with MEF-conditioned medium (CM + MCT1i >10k) for 5 days. MEF-conditioned medium was separated into fractions using centrifugal filters of size 10 kDa. Because the retentate is concentrated following filtration, it was reconstituted to the starting volume by the addition of basal medium. Error bars indicate ± 1 SEM of biological replicates (n = 3). ns: not significant; *** $p < 0.001$.

FUTURE DIRECTIONS

Here we discuss continuing work on human pluripotent stem cell metabolism that has stemmed from the findings in this dissertation.

Understanding the role of N-MYC in naive pluripotency

We have shown that naive hESCs exhibit increased glycolytic flux, MYC transcriptional activity, and nuclear N-MYC localization relative to primed hESCs. Our data on human blastocysts also confirm the increased MYC transcriptional activity and nuclear N-MYC levels. In addition, N-MYC seems to be more closely associated with naive pluripotency in both human and mouse, while C-MYC coincides with glycolytic phenotype. C-MYC has a well-established role in promoting glycolysis in proliferating cells, and our data suggest that N-MYC is important for human naive pluripotency. One interesting question is whether N-MYC simply acts as a redundant transcription factor to C-MYC in promoting glycolysis, or N-MYC and C-MYC bind to unique sets of target genes and regulate transcriptional activity in distinctive ways. There are a couple of interesting experiments to address this question: one is to perform chromatin immunoprecipitation with DNA sequencing (ChIP-Seq) to examine whether N-MYC and C-MYC bind to different sets of target genes in naive hESCs; the other is to perform immunoprecipitation (IP) to determine whether N-MYC and C-MYC recruit different partner proteins, such as Max and Miz-1(Adhikary and Eilers, 2005), to form different MYC complexes in naive hESCs.

Investigating the interplay between metabolism and epigenetics in naive and primed human pluripotent stem cells

One of the characteristics of human preimplantation development is genome-wide reduction in DNA methylation (Guo et al., 2014). Naive human pluripotent stem cells generated by 5i/LAF method also have decreased global DNA methylation in both CpG (26.9% - 33.2%) and non-CpG contexts (0.19% - 0.29%), compared to their primed counterparts (CpG, 75.2% - 81.0%; non-CpG, 0.32% - 0.60%) (Theunissen et al., 2014). The de-methylation in naive cells and re-methylation in primed cells at such a great scale likely accompany significant changes in cellular metabolism, for that both de-methylation and re-methylation processes post high demand on metabolites, cofactors, and even metabolic enzymes. For example, during DNA methylation, DNA methyltransferases (DNMTs) add a methyl group from S-adenosyl methionine (SAM) to the substrate, DNA, and as a result form the byproduct S-adenosyl homocysteine (SAH). The complexity of SAM and SAH metabolism (Selhub and Miller, 1992) suggests that the metabolism of pluripotent stem cells is probably tightly regulated during early embryo development according to the vast change of the methylome. It has also been shown that dietary intake of methyl donors can affect levels DNA methylation (Feil and Fraga, 2012), therefore, it would be very interesting in the future to determine whether metabolic inputs can affect the methylome of pluripotent stem cells, and if so, whether the change in DNA methylation caused by metabolic manipulation can in turn affect the stage of pluripotency (for example, naive versus primed).

Understanding the mechanism by which MCT1 inhibition causes proliferative defects in feeder-free primed hESCs

We have demonstrated that we can effectively reduce glycolysis in feeder-free naive hESCs, feeder-supported and feeder-free primed hESCs by using a small molecule inhibitor

towards MCT1. And glycolysis inhibition by MCT1 causes a proliferative impairment in feeder-supported naive hESCs and feeder-supported primed hESCs, without affecting the proliferation of feeder-supported primed hESCs. The mechanistic link between glycolysis inhibition and proliferative impairment in hESCs is unknown. We have tried to use various metabolites to supplement the culture medium of MCT1 inhibitor-treated, feeder-free primed hESCs, and see whether a specific metabolite can rescue the proliferative defect caused by MCT1 inhibition in feeder-free primed hESCs. So far, we have found that supplementing the culture medium with uridine has a minor and partial rescuing effect, which is consistent with our hypothesis that feeder-free primed hESCs rely on glycolysis for nucleotide biosynthesis, and reduction of glycolysis causes decreased nucleotide biosynthesis and thus reduced proliferation. In the future, more work needs to be done to test whether other anabolic intermediates have similar rescuing effect, and whether a combination of those metabolites result in a fuller rescue.

The Hippo signaling pathway might be involved in the mechanism by which MCT1 inhibition affects the proliferation of feeder-free primed hESCs. Our preliminary data indicate that the nuclear YAP levels decrease upon 5-day MCT1 inhibitor treatment in feeder-free primed hESCs compared with DMSO-treated cells. Consistently, whole-genome mRNA microarray data show that the expression levels of two YAP target genes, connective tissue growth factor (CTGF) and cysteine-rich angiogenic inducer 61 (CYP61), both of which are important for cell growth (Zhao et al., 2008; Cheng et al., 2015), decrease upon 5-day MCT1 inhibitor treatment in feeder-free primed hESCs. Together, these data suggest that the decreased glycolytic metabolism caused by MCT1 inhibition might reduce nuclear YAP levels, down-regulate the expression of YAP target genes, CTGF and CYP61, and thus negatively affect the proliferation rate of feeder-free primed hESCs. In the future, we would test this hypothesis by

pharmacologically inhibiting YAP transcriptional activity (Liu-Chittenden et al., 2012) and see whether the proliferation rate is decreased in feeder-free primed hESCs, and by genetically overexpressing YAP or CTGF or CYP61 and see whether the proliferation rate can be restored in MCT1 inhibitor-treated feeder-free primed hESCs.

Identifying the protein factor(s) responsible for reprogramming primed hESC metabolism to a state less reliant on glycolysis for anabolism

Our findings suggest that feeder-supported and feeder-free primed hESCs metabolize glucose differently, and feeder-free primed hESCs may rely on glucose more for biosynthetic pathways that support proliferation. Moreover, we have shown that the above 10kDa protein factor(s) secreted by MEFs can potentially reduce the reliance of primed hESCs on glucose for proliferation. We have conducted mass-spectrometry based protein identification of MEF-conditioned medium, and have identified many candidate proteins that are uniquely present in MEF-conditioned medium versus blank culture medium or FF hESC-conditioned medium. Among these candidate proteins, PAI1 has been reported previously to be important for the growth and hESCs. However, we have found that PAI1 alone is not sufficient to rescue the proliferation impairment in MCT1 inhibited feeder-free primed hESCs. So far, we are unable to identify a combination of protein factors that are responsible for reprogramming hESC metabolism and making them less reliant on glucose for proliferation. In the future, an unbiased method to assess the rescuing effect of a combination of candidate proteins may uncover the factors necessary for regulating hESC metabolism, and will be beneficial for identifying ideal culture conditions for hESCs *in vitro*.

Metabolic manipulation as a tool for lineage differentiation of pluripotent stem cells

We have demonstrated that manipulation of metabolism can promote a particular cell fate. More specifically, we show that glycolysis inhibition induces neural progenitor specification in feeder-free primed hESCs. It is possible that other types of metabolic modulation can also guide hESCs differentiate into other specific lineages. Interestingly, Tohyama et al. (Tohyama et al., 2013) cultured mouse and human PSC derivatives with glucose-depleted, lactate-rich culture medium and found that only cardiomyocytes survived, up to 99% purity, suggesting that a biochemical strategy could greatly facilitate the generation of certain cell types useful for regenerative medicine while eliminating the potentially tumorigenic pluripotent stem cells. Therefore, better understanding the metabolic differences between pluripotent stem cells and various differentiated cell types, including their unique dependence on certain nutrients and differential expression of specific metabolic enzymes, could yield key information on how to use metabolic manipulation to promote lineage differentiation of pluripotent stem cells for therapeutic purposes.

EXPERIMENTAL PROCEDURES

Cell Culture

Conventional feeder-supported human ESC lines H1, H9 (WiCell Research Institute, Inc., Madison, WI), HSF1 (University of California San Francisco, San Francisco, CA), UCLA1, and UCLA9 (University of California Los Angeles, Los Angeles, CA) were maintained on radiation inactivated MEF feeder layers (GlobalStem) and passed enzymatically by treatment for 2 min with 1 mg/ml Collagenase type IV (STEMCELL Technologies), and then mechanically lifted by using a cell scraper (Falcon), followed by passing through a 100-μm cell strainer. Conventional feeder-supported human ESCs were cultured in human ESC medium (hESM) – DMEM/F12 (Invitrogen) supplemented with 20% KSR (Invitrogen), 1% nonessential amino acids (NEAA, Invitrogen), 0.1 mM β-mercaptoethanol (Invitrogen), and 10 ng/ml FGF2 (Peprotech). Primed feeder-free human ESC lines H1, H9, and HSF1 were cultured on plates pre-coated with 1:25 diluted Matrigel (BD Biosciences) in mTeSR1 medium (STEMCELL Technologies). Tissue culture media were filtered using a low protein-binding 0.22 μm filter (Millipore). All experiments were performed under 5% CO_2 and atmospheric oxygen levels.

Naive human pluripotent stem cells were generated and maintained using the 5i/LAF condition exactly as described (Theunissen et al., 2014). Briefly, feeder-supported UCLA1 and UCLA9 hESCs were grown to ~ 60% density and fed hESM supplemented with 10 μM ROCK inhibitor Y-27632 (Stemgent). The following day, hESCs were trypsinized to single cell (0.05% Trypsin, ThermoFisher Scientific) and plated on feeders at 2 x 10^5 cells/well of a 6-well dish in hESM with ROCKi. Two days later culture medium was switched to 5i/LAF (1 μM PD0325901, 10 μM Y-27632 (Stemgent), 1 μM IM-12 (Enzo), 0.5 μM SB590885 (R&D), 1 μM WH-4-023 (A Chemtek), 20 ng/ml recombinant hLIF (Millipore), 20 ng/ml Activin A (Peprotech), and 8 ng/ml

FGF2 (R&D) in a 1:1 mixture of DMEM/F12 and Neurobasal medium (Invitrogen) supplemented with 1x N2, B27, NEAA, Pen/Strep, Glutamine (Invitrogen), 0.1 mM beta-mercaptoethanol, 0.5% KSR and 50 μg/ml BSA). Medium was changed daily, and in 8-10 days, after massive cell death, several dome-shaped colonies appeared. These colonies were passaged using Accutase (ThermoFisher Scientific). After 3-4 passages naive hESCs had expanded enough to be split at 1:4 or 1:5 ratio every 5 days. Before plating cells were passed through 40-μm mesh since naive hESCs grow best when plated as single cells. Feeder-supported naive line UCLA19 was derived directly from the inner cell mass of a human blastocyst and since cultured in 5i/LAF medium.

Another naive human pluripotent stem cell line, H9 reset, was maintained using the Takashima et al. method exactly as described (Takashima et al., 2014), and cultured in an incubator with 5% O_2 and 5% CO_2 at 37 °C. For comparing the glycolytic rates in reset versus primed H9 hESCs, both reset and primed cells were received from the Austin Smith Lab and cultured under 5% O_2 condition.

Neural rosette differentiation was induced by treatment with DMEM/F12 supplemented with B27 and N2 (Gibco), 1 μM retinoic acid (Sigma), 20 ng/ml FGF2, and 1 μM purmorphamine (Cayman chemical) for 10 days.

Cells were treated with AZD3965 (AstraZeneca, 250 nM) or CD532 (Millipore, 25 – 250 nM) for indicated times to assess the effects of MCT1 inhibition or N-MYC inhibition.

Immunostaining of Human Preimplantation Embryos

All experiments were performed using human embryos that were excess to infertility treatment and donated for research following informed consent in accordance with the guidelines

established by UCLA Embryonic Stem Cell Research Oversight (ESCRO) Committee and the Committee on the Use of Human Subjects Institutional Review Board (IRB).

Human blastocysts were thawed using Vit Kit-Thaw (Irvine Scientific) according to manufacturer protocol. The embryos were cultured in drops of Continuous Single Culture medium (Irvine Scientific) supplemented with 20% Quinn's Advantage SPS Serum Protein Substitute (Sage Media) under mineral oil (Irvine Scientific) overnight at 37 °C, 6% CO_2 and 5% O_2. Embryos were fixed at room temperature in 4% paraformaldehyde for 30 minutes, and then washed several times in 0.1% Tween-20 in PBS. Embryos were permeabilized in 1% Tween-20 in PBS at 4 °C for 4 days on a rotating shaker and then blocked in 10% FBS and 0.2% Tween-20 in PBS at room temperature for 1 hour. Embryos were incubated in a 1:100 dilution of primary antibody in blocking buffer at 4°C overnight on a rotating shaker and washed several times in 0.1% Tween-20 in PBS at room temperature. Embryos were incubated in a 1:500 dilution of secondary antibody anti-rabbit Alexa Fluor 555 (Invitrogen) in blocking buffer at room temperature for 1 hour while protected from light. They were then washed several times in 0.1% Tween-20 in PBS and mounted in ProLong Diamond with DAPI (Invitrogen) on a glass slide, covered with a glass coverslip and left at room temperature to cure overnight. Images were taken using a LSM780 confocal microscope (Zeiss).

Glucose Consumption and Lactate Production Rates

Cellular glucose consumption and lactate export rates were measured using a Nova Biomedical BioProfile Basic Analyzer. Briefly, cells were seeded in triplicates in 6-well plates at usual passing density. Ninety-six hours post-seeding, when the colonies were subconfluent, cells were washed with PBS, and 1ml fresh medium was added to each well, including an empty well

without any cells as a blank control. After 24-hour incubation, culture medium was collected and then analyzed by the Nova BioProfile analyzer. Cell numbers were determined both before and after the 24-hour incubation period using a Coulter particle analyzer and used to normalize the calculated rates.

Among different figures, the same cell line might show different values in glucose and lactate readings, which is due to the difference in cell numbers between different experiments. Since plating density of cells can impact metabolism, we always ensure that different treatment groups or cell lines within a given experiment have similar cell counts when glucose and lactate measurements are taken. We accomplish this by plating hESCs at different densities and measuring the media glucose and lactate amounts in the ones with similar cell counts.

Oxygen Consumption Rates

For comparing oxygen consumption rates in feeder-supported hESCs, cells were treated with Accutase (Invitrogen) for 5 minutes after PBS wash, passed through a 40-μm cell strainer (BD), and cell count was obtained. Four million cells were spun down at 300g for 5 minutes, resuspended in 250 μl culture medium, and transferred to an anaerobic chamber of 250 μl volume. The anaerobic chamber was maintained at 37 °C by a water circulating system (DC10, Thermo), and fitted with a fiber optic oxygen sensor (Model 110, INSTECH). Oxygen concentration was sensed by the quenching of fluorescence of an indicator dye trapped in a matrix at the tip of the probe, and was calibrated with 15 mM sodium hydrosulfite (Sigma) and cell culture media, corresponding to 0% and 20.9% oxygen respectively.

Extracellular Acidification and Oxygen Consumption Rates

For comparing extracellular acidification and oxygen consumption rates in feeder-free primed hESCs, with AZD3965 or DMSO treatment, cells were seeded onto an XF24 Cell Culture Microplate (Seahorse Bioscience) at 2 - 7.5 × 10^4 cells/well with the 10 μM ROCK inhibitor Y-27632 (Calbiochem) and incubated at 37°C overnight. Extracellular acidification and oxygen consumption rates were measured by using an XF24 Extracellular Flux Analyzer (Seahorse Bioscience) in unbuffered DMEM assay medium supplemented with 1mM pyruvate and 25mM glucose after 45 to 60-minute equilibration, and were normalized to protein concentration using the Protein Assay reagent (Bio-Rad).

Mass Spectrometry-based Metabolomics Analysis

Cells were incubated in medium containing 3.151 g/l 1,2-^{13}C-glucose for 24 hours. The following day, cells were rinsed with cold 150 mM ammonium acetate (NH_4AcO). Cells were carefully scraped off in 800 μl of 50% ice cold methanol. An internal standard of 12.5 μM norvaline was added to the cell suspension, followed by 400 μl of cold chloroform. After vortexing for 15 min, the aqueous layer was transferred to a glass vial and the metabolites were dried under vacuum. Metabolites were resuspended in 100 μl 70% acetonitrile (ACN) and 5 μl of this solution was used for the mass spectrometer- based analysis. The analysis was performed on a Q Exactive (Thermo Scientific) in polarity-switching mode with positive voltage 3.0 kV and negative voltage 2.25 kV. The mass spectrometer was coupled to an UltiMate 3000RSLC (Thermo Scientific) UHPLC system. Mobile phase A was 5 mM NH_4AcO, pH 9.9, B was ACN, and the separation achieved on a Luna 3mm NH_2 100A (150 x 2.0 mm) (Phenomenex) column. The flow was 300 μl/min, and the gradient ran from 15% A to 95% A in 18 min, followed by an isocratic step for 9 minutes and re-equilibration for 7 minutes. Metabolites were detected and

quantified as area under the curve (AUC) based on retention time and accurate mass (≤ 3 ppm) using the TraceFinder 3.1 (Thermo Scientific) software. Relative amounts of metabolites between various conditions, as well as percentage of labeling were calculated and corrected for naturally occurring ^{13}C abundance (Yuan et al., 2008; Moseley, 2010). For the heatmap depiction of the relative amounts of glycolytic intermediates, Z scores were calculated by subtracting the mean value across all samples, then dividing over standard deviation (SD). When feeder-supported and feeder-free primed hESCs were compared, a plate of irradiated MEFs without hESCs was also labeled with 1,2-^{13}C-glucose, and traced the incorporation of ^{13}C into downstream glucose metabolites using LC-MS, to control for the presence of feeder cells in the FS conditions (Figure S4E-H, and Fan et al., 2014; Yuan et al., 2008).

Immunoblot Assays

For preparing whole cell lysates, cells were lysed in M-PER Mammalian Protein Extraction Reagent (Thermo) with 20 mM NaF, 1 mM Na_3VO_4, 4 μg/ml aprotinin, 4 μg/ml leupeptin, 4 μg/ml pepstatin, and 1 mM DTT. Nuclear and cytoplasmic fractions were prepared using the following protocol: Buffer A, containing 10 mM HEPES (pH 7.9), 10 mM KCl, 0.1 mM EDTA, 0.4% NP40, 20 mM NaF, 1 mM Na_3VO_4, 4 μg/ml aprotinin, 4 μg/ml leupeptin, 4 μg/ml pepstatin, and 1 mM DTT, was used to extract cytoplasmic proteins; Nuclear pellet was resuspended in Buffer B, which contains 20 mM HEPES (pH 7.9), 400 mM NaCl, 1mM EDTA, 10% glycerol, 20 mM NaF, 1 mM Na_3VO_4, 4 μg/ml aprotinin, 4 μg/ml leupeptin, 4 μg/ml pepstatin, and 1 mM DTT, and placed on vortex at 4 °C for 2 hours to extract nuclear proteins. Western blot analysis was carried out according to standard methods. Protein concentrations of cell extracts were determined by using the Protein Assay reagent (Bio-Rad). The following

commercial antibodies were used as probes: C-MYC, N-MYC, OCT4A, TBP (Cell Signaling), β-Tubulin (Sigma), MCT1, and GAPDH (Abcam).

RNA-Seq

Feeder-supported UCLA1 primed and naive hESCs were cultured in a 6-well dish. Primed hESCs were harvested with 1mg/ml Collagenase IV (Life Technologies) for 8min at 37 °C, or until the edges of colonies lifted off slightly. Colonies were collected in hESM followed by sequential sedimentation steps to deplete feeder cells. Colonies were then washed once in PBS and collected in 1ml Trizol (Invitrogen). Naive hESCs were feeder depleted by treating the cells with Accutase and passing the cells through a 40-μm mesh. Under these conditions feeder cells do not separate into single cells and therefore do not pass through the filter. Cells were collected in 1 ml Trizol after a PBS wash. Total RNA was isolated by phenol chloroform extraction and purified by RNeasy Mini Kit (Qiagen). The TruSeq Stranded mRNA Library Prep Kit (Illumina) was used to prepare mRNA libraries following manufacturer's instructions. The libraries were run on 2% SeaPlaque Agarose gel (Lonza) to remove primer contaminants, and purified using MinElute Gel Extraction Kit (Qiagen). Final library amounts were quantified by Qubit dsDNA HS Assay (Invitrogen) and sequenced on Illumina HiSeq 2500 instrument at the UCLA High-Throughput Sequencing Facility. Reads were mapped to hg19 assembly of the human genome using the TopHat read-mapping algorithm (Trapnell et al., 2009), and gene expression levels were calculated as RPKM values (Mortazavi et al., 2008).

Microarray and Enrichment Analysis

Total RNA was isolated by using the Absolutely RNA kit (Stratagene) and reverse-transcribed with the SuperScript III First-Strand Synthesis System (Invitrogen) with oligo dT primers. Whole-genome expression analysis was performed with the HG-U133 plus 2 array (Affymetrix) at the UCLA Clinical Microarray Core.

Gene Set Enrichment Analysis (Subramanian et al., 2005) was performed using the Molecular Signatures Database (MSigDB) C2 collection (version 5.0) of canonical signaling pathways, cellular processes, chemical and genetic perturbations, and human disease states. For GSEA on primed hESCs with AZD3965 or DMSO treatment, readings of probe sets were first RMA normalized, and then collapsed according to the probes with maximum expression values into gene symbols, which were then ranked according to the log10 p value from paired t-test between AZD3965 and DMSO groups in three hESC lines: H1, H9, and HSF1. Pre-ranked GSEA was also conducted on naive and primed UCLA1 hESCs.

For human preimplantation datasets, each data was analyzed separately. The mRNA microarray dataset by Vassena et al., 2011(GEO accession: GSE29397), was processed using Bioconductor package in R, normalized using the RMA method, and then imported to GSEA. The single-cell RNA-Seq dataset by Yan et al., 2013 (GEO accession: GSE36552) contained the gene expression levels presented as RPKM values, based on which the log fold changes (base 2) were calculated and ranked to generate an ordered gene list for Pre-ranked GSEA.

For the enriched MYC-regulated gene sets identified by GSEA, MENSSEN_MYC_TARGETS was first reported by Menssen et al. (Menssen and Hermeking, 2002), SCHLOSSER_MYC_TARGETS_REPRESSED_BY_SERUM was based on published data by Schlosser et al. (Schlosser et al., 2005), and DANG_MYC_TARGETS_UP was reported by

Zeller et al. (Zeller et al., 2003). Details about each gene set can also be found at http://software.broadinstitute.org/gsea/msigdb/.

A web-based application GOrilla (Eden et al., 2009) was used to identify enriched Gene Ontology (Ashburner et al., 2000) terms in a ranked list of all genes according to the differential expression in AZD3965 versus DMSO-treated H1, H9, and HSF1 hESCs.

Cell Proliferation

Cells were seeded in triplicates in 6-well plates, and cell counts were obtained using a Coulter particle analyzer 5 days after seeding.

REFERENCES

Adhikary, S., and Eilers, M. (2005). Transcriptional regulation and transformation by Myc proteins. Nat. Rev. Mol. Cell Biol. *6*, 635–645.

Adijanto, J., and Philp, N.J. (2012). Chapter Nine - The SLC16A Family of Monocarboxylate Transporters (MCTs)—Physiology and Function in Cellular Metabolism, pH Homeostasis, and Fluid Transport. In Current Topics in Membranes, M.O. Bevensee, ed. (Academic Press), pp. 275–312.

Anastasiou, D., Yu, Y., Israelsen, W.J., Jiang, J.-K., Boxer, M.B., Hong, B.S., Tempel, W., Dimov, S., Shen, M., Jha, A., et al. (2012). Pyruvate kinase M2 activators promote tetramer formation and suppress tumorigenesis. Nat. Chem. Biol. *8*, 839–847.

Anderson, V.E., Weiss, P.M., and Cleland, W.W. (1984). Reaction intermediate analogues for enolase. Biochemistry (Mosc.) *23*, 2779–2786.

Ashburner, M., Ball, C.A., Blake, J.A., Botstein, D., Butler, H., Cherry, J.M., Davis, A.P., Dolinski, K., Dwight, S.S., Eppig, J.T., et al. (2000). Gene Ontology: tool for the unification of biology. Nat. Genet. *25*, 25–29.

Bendall, S.C., Hughes, C., Campbell, J.L., Stewart, M.H., Pittock, P., Liu, S., Bonneil, E., Thibault, P., Bhatia, M., and Lajoie, G.A. (2009). An enhanced mass spectrometry approach reveals human embryonic stem cell growth factors in culture. Mol. Cell. Proteomics MCP *8*, 421–432.

Bensinger, S.J., and Christofk, H.R. (2012). New aspects of the Warburg effect in cancer cell biology. Semin. Cell Dev. Biol. *23*, 352–361.

Buhr, N., Carapito, C., Schaeffer, C., Hovasse, A., Van Dorsselaer, A., and Viville, S. (2007). Proteome analysis of the culture environment supporting undifferentiated mouse embryonic stem and germ cell growth. Electrophoresis *28*, 1615–1623.

Chambers, S.M., Fasano, C.A., Papapetrou, E.P., Tomishima, M., Sadelain, M., and Studer, L. (2009). Highly efficient neural conversion of human ES and iPS cells by dual inhibition of SMAD signaling. Nat. Biotechnol. *27*, 275–280.

Chan, Y.-S., Göke, J., Ng, J.-H., Lu, X., Gonzales, K.A.U., Tan, C.-P., Tng, W.-Q., Hong, Z.-Z., Lim, Y.-S., and Ng, H.-H. (2013). Induction of a Human Pluripotent State with Distinct Regulatory Circuitry that Resembles Preimplantation Epiblast. Cell Stem Cell *13*, 663–675.

Cheng, G., Zhang, H., Zhang, L., and Zhang, J. (2015). Cyr61 promotes growth of glioblastoma in vitro and in vivo. Tumour Biol. J. Int. Soc. Oncodevelopmental Biol. Med. *36*, 2869–2873.

Chin, A.C.P., Fong, W.J., Goh, L.-T., Philp, R., Oh, S.K.W., and Choo, A.B.H. (2007). Identification of proteins from feeder conditioned medium that support human embryonic stem cells. J. Biotechnol. *130*, 320–328.

Christofk, H.R., Vander Heiden, M.G., Harris, M.H., Ramanathan, A., Gerszten, R.E., Wei, R., Fleming, M.D., Schreiber, S.L., and Cantley, L.C. (2008). The M2 splice isoform of pyruvate kinase is important for cancer metabolism and tumour growth. Nature *452*, 230–233.

Chung, S., Arrell, D.K., Faustino, R.S., Terzic, A., and Dzeja, P.P. (2010). Glycolytic network restructuring integral to the energetics of embryonic stem cell cardiac differentiation. J. Mol. Cell. Cardiol. *48*, 725–734.

Consortium, T.I.S.C.I., Akopian, V., Andrews, P.W., Beil, S., Benvenisty, N., Brehm, J., Christie, M., Ford, A., Fox, V., Gokhale, P.J., et al. (2010). Comparison of defined culture systems for feeder cell free propagation of human embryonic stem cells. Vitro Cell. Dev. Biol. - Anim. *46*, 247–258.

Critchlow, S.E., Hopcroft, L., Mooney, L., Curtis, N., Whalley, N., Zhong, H., Logie, A., Revill, M., Xie, L., Zhang, J., et al. (2012). Abstract 3224: Pre-clinical targeting of the metabolic phenotype of lymphoma by AZD3965, a selective inhibitor of monocarboxylate transporter 1 (MCT1). Cancer Res. *72*, 3224–3224.

Denko, N.C. (2008). Hypoxia, HIF1 and glucose metabolism in the solid tumour. Nat. Rev. Cancer *8*, 705–713.

Doherty, J.R., Yang, C., Scott, K.E.N., Cameron, M.D., Fallahi, M., Li, W., Hall, M.A., Amelio, A.L., Mishra, J.K., Li, F., et al. (2014). Blocking Lactate Export by Inhibiting the Myc Target MCT1 Disables Glycolysis and Glutathione Synthesis. Cancer Res. *74*, 908–920.

Eden, E., Navon, R., Steinfeld, I., Lipson, D., and Yakhini, Z. (2009). GOrilla: a tool for discovery and visualization of enriched GO terms in ranked gene lists. BMC Bioinformatics *10*, 48.

Eiges, R., Schuldiner, M., Drukker, M., Yanuka, O., Itskovitz-Eldor, J., and Benvenisty, N. (2001). Establishment of human embryonic stem cell-transfected clones carrying a marker for undifferentiated cells. Curr. Biol. *11*, 514–518.

Fan, J., Ye, J., Kamphorst, J.J., Shlomi, T., Thompson, C.B., and Rabinowitz, J.D. (2014). Quantitative flux analysis reveals folate-dependent NADPH production. Nature *510*, 298–302.

Feil, R., and Fraga, M.F. (2012). Epigenetics and the environment: emerging patterns and implications. Nat. Rev. Genet. *13*, 97–109.

Folmes, C.D., Arrell, D.K., Zlatkovic-Lindor, J., Martinez-Fernandez, A., Perez-Terzic, C., Nelson, T.J., and Terzic, A. (2013). Metabolome and metaboproteome remodeling in nuclear reprogramming. Cell Cycle *12*, 2355–2365.

Folmes, C.D.L., Nelson, T.J., Martinez-Fernandez, A., Arrell, D.K., Lindor, J.Z., Dzeja, P.P., Ikeda, Y., Perez-Terzic, C., and Terzic, A. (2011). Somatic Oxidative Bioenergetics Transitions into Pluripotency-Dependent Glycolysis to Facilitate Nuclear Reprogramming. Cell Metab. *14*, 264–271.

Folmes, C.D.L., Martinez-Fernandez, A., Faustino, R.S., Yamada, S., Perez-Terzic, C., Nelson, T.J., and Terzic, A. (2012a). Nuclear Reprogramming with c-Myc Potentiates Glycolytic Capacity of Derived Induced Pluripotent Stem Cells. J Cardiovasc. Transl. Res. *6*, 10–21.

Folmes, C.D.L., Nelson, T.J., Dzeja, P.P., and Terzic, A. (2012b). Energy metabolism plasticity enables stemness programs. Ann. N. Y. Acad. Sci. *1254*, 82–89.

Gafni, O., Weinberger, L., Mansour, A.A., Manor, Y.S., Chomsky, E., Ben-Yosef, D., Kalma, Y., Viukov, S., Maza, I., Zviran, A., et al. (2013). Derivation of novel human ground state naive pluripotent stem cells. Nature *504*, 282–286.

Gefflaut, T., Blonski, C., and Périé, J. (1996). Slow reversible inhibitions of rabbit muscle aldolase with substrate analogues: synthesis, enzymatic kinetics and UV difference spectroscopy studies. Bioorg. Med. Chem. *4*, 2043–2054.

Guile, S.D., Bantick, J.R., Cheshire, D.R., Cooper, M.E., Davis, A.M., Donald, D.K., Evans, R., Eyssade, C., Ferguson, D.D., Hill, S., et al. (2006). Potent blockers of the monocarboxylate transporter MCT1: Novel immunomodulatory compounds. Bioorg. Med. Chem. Lett. *16*, 2260–2265.

Guo, H., Zhu, P., Yan, L., Li, R., Hu, B., Lian, Y., Yan, J., Ren, X., Lin, S., Li, J., et al. (2014). The DNA methylation landscape of human early embryos. Nature *511*, 606–610.

Gustafson, W.C., Meyerowitz, J.G., Nekritz, E.A., Chen, J., Benes, C., Charron, E., Simonds, E.F., Seeger, R., Matthay, K.K., Hertz, N.T., et al. (2014). Drugging MYCN through an Allosteric Transition in Aurora Kinase A. Cancer Cell *26*, 414–427.

Halestrap, A.P. (2011). Monocarboxylic Acid Transport. In Comprehensive Physiology, (John Wiley & Sons, Inc.),.

Harris, J.I., and Waters, M. (1976). 1 Glyceraldehyde-3-phosphate Dehydrogenase. In The Enzymes, P.D. Boyer, ed. (Academic Press), pp. 1–49.

Jeon, Y.K., Yoo, D.R., Jang, Y.H., Jang, S.Y., and Nam, M.J. (2011). Sulforaphane induces apoptosis in human hepatic cancer cells through inhibition of 6-phosphofructo-2-kinase/fructose-2,6-biphosphatase4, mediated by hypoxia inducible factor-1-dependent pathway. Biochim. Biophys. Acta *1814*, 1340–1348.

Lim, J.W.E., and Bodnar, A. (2002). Proteome analysis of conditioned medium from mouse embryonic fibroblast feeder layers which support the growth of human embryonic stem cells. Proteomics *2*, 1187–1203.

Liu-Chittenden, Y., Huang, B., Shim, J.S., Chen, Q., Lee, S.-J., Anders, R.A., Liu, J.O., and Pan, D. (2012). Genetic and pharmacological disruption of the TEAD-YAP complex suppresses the oncogenic activity of YAP. Genes Dev. *26*, 1300–1305.

Locasale, J.W. (2013). Serine, glycine and one-carbon units: cancer metabolism in full circle. Nat. Rev. Cancer *13*, 572–583.

Lu, J., Hou, R., Booth, C.J., Yang, S.-H., and Snyder, M. (2006). Defined culture conditions of human embryonic stem cells. Proc. Natl. Acad. Sci. *103*, 5688–5693.

Ludwig, T.E., Levenstein, M.E., Jones, J.M., Berggren, W.T., Mitchen, E.R., Frane, J.L., Crandall, L.J., Daigh, C.A., Conard, K.R., Piekarczyk, M.S., et al. (2006). Derivation of human embryonic stem cells in defined conditions. Nat. Biotechnol. *24*, 185–187.

Mann, W.R., Dragland, C.J., Vinluan, C.C., Vedananda, T.R., Bell, P.A., and Aicher, T.D. (2000). Diverse mechanisms of inhibition of pyruvate dehydrogenase kinase by structurally distinct inhibitors. Biochim. Biophys. Acta *1480*, 283–292.

Marks, H., Kalkan, T., Menafra, R., Denissov, S., Jones, K., Hofemeister, H., Nichols, J., Kranz, A., Francis Stewart, A., Smith, A., et al. (2012). The Transcriptional and Epigenomic Foundations of Ground State Pluripotency. Cell *149*, 590–604.

Mcharg, J., and Littlechild, J.A. (1996). Studies with inhibitors of the glycolytic enzyme phosphoglycerate kinase for potential treatment of cardiovascular and respiratory disorders. J. Pharm. Pharmacol. *48*, 201–205.

Meng, M., Chane, T.L., Sun, Y.J., and Hsiao, C.D. (1999). Probing the location and function of the conserved histidine residue of phosphoglucose isomerase by using an active site directed inhibitor N-bromoacetylethanolamine phosphate. Protein Sci. Publ. Protein Soc. *8*, 2438–2443.

Menssen, A., and Hermeking, H. (2002). Characterization of the c-MYC-regulated transcriptome by SAGE: Identification and analysis of c-MYC target genes. Proc. Natl. Acad. Sci. *99*, 6274–6279.

Minutolo, F., Macchia, M., Katzenellenbogen, B.S., and Katzenellenbogen, J.A. (2011). Estrogen receptor β ligands: recent advances and biomedical applications. Med. Res. Rev. *31*, 364–442.

Mortazavi, A., Williams, B.A., McCue, K., Schaeffer, L., and Wold, B. (2008). Mapping and quantifying mammalian transcriptomes by RNA-Seq. Nat. Methods *5*, 621–628.

Moseley, H.N. (2010). Correcting for the effects of natural abundance in stable isotope resolved metabolomics experiments involving ultra-high resolution mass spectrometry. BMC Bioinformatics *11*, 139.

Murray, C.M., Hutchinson, R., Bantick, J.R., Belfield, G.P., Benjamin, A.D., Brazma, D., Bundick, R.V., Cook, I.D., Craggs, R.I., Edwards, S., et al. (2005). Monocarboxylate transporter MCT1 is a target for immunosuppression. Nat. Chem. Biol. *1*, 371–376.

Niakan, K.K., and Eggan, K. (2013). Analysis of human embryos from zygote to blastocyst reveals distinct gene expression patterns relative to the mouse. Dev. Biol. *375*, 54–64.

Nichols, J., and Smith, A. (2009). Naive and Primed Pluripotent States. Cell Stem Cell *4*, 487–492.

Pannell, D., Osborne, C.S., Yao, S., Sukonnik, T., Pasceri, P., Karaiskakis, A., Okano, M., Li, E., Lipshitz, H.D., and Ellis, J. (2000). Retrovirus vector silencing is de novo methylase independent and marked by a repressive histone code. EMBO J. *19*, 5884–5894.

Pastor, W.A., Chen, D., Liu, W., Kim, R., Sahakyan, A., Lukianchikov, A., Plath, K., Jacobsen, S.E., and Clark, A.T. (2016). Naive Human Pluripotent Cells Feature a Methylation Landscape Devoid of Blastocyst or Germline Memory. Cell Stem Cell *18*, 323–329.

Peiffer, I., Barbet, R., Zhou, Y.-P., Li, M.-L., Monier, M.-N., Hatzfeld, A., and Hatzfeld, J.A. (2008). Use of Xenofree Matrices and Molecularly-Defined Media to Control Human Embryonic Stem Cell Pluripotency: Effect of Low Physiological TGF-β Concentrations. Stem Cells Dev. *17*, 519–534.

Penso, J., and Beitner, R. (1998). Clotrimazole and bifonazole detach hexokinase from mitochondria of melanoma cells. Eur. J. Pharmacol. *342*, 113–117.

Petropoulos, S., Edsgärd, D., Reinius, B., Deng, Q., Panula, S.P., Codeluppi, S., Plaza Reyes, A., Linnarsson, S., Sandberg, R., and Lanner, F. (2016). Single-Cell RNA-Seq Reveals Lineage and X Chromosome Dynamics in Human Preimplantation Embryos. Cell *165*, 1012–1026.

Polanski, R., Hodgkinson, C.L., Fusi, A., Nonaka, D., Priest, L., Kelly, P., Trapani, F., Bishop, P.W., White, A., Critchlow, S.E., et al. (2014). Activity of the Monocarboxylate Transporter 1 Inhibitor AZD3965 in Small Cell Lung Cancer. Clin. Cancer Res. *20*, 926–937.

Prigione, A., Fauler, B., Lurz, R., Lehrach, H., and Adjaye, J. (2010). The Senescence-Related Mitochondrial/Oxidative Stress Pathway is Repressed in Human Induced Pluripotent Stem Cells. STEM CELLS *28*, 721–733.

Prowse, A.B.J., McQuade, L.R., Bryant, K.J., Van Dyk, D.D., Tuch, B.E., and Gray, P.P. (2005). A proteome analysis of conditioned media from human neonatal fibroblasts used in the maintenance of human embryonic stem cells. Proteomics *5*, 978–989.

Prowse, A.B.J., McQuade, L.R., Bryant, K.J., Marcal, H., and Gray, P.P. (2007). Identification of potential pluripotency determinants for human embryonic stem cells following proteomic analysis of human and mouse fibroblast conditioned media. J. Proteome Res. *6*, 3796–3807.

Rabinowitz, J.D., and Vastag, L. (2012). Teaching the design principles of metabolism. Nat. Chem. Biol. *8*, 497–501.

Rajala, K., Lindroos, B., Hussein, S.M., Lappalainen, R.S., Pekkanen-Mattila, M., Inzunza, J., Rozell, B., Miettinen, S., Narkilahti, S., Kerkelä, E., et al. (2010). A Defined and Xeno-Free Culture Method Enabling the Establishment of Clinical-Grade Human Embryonic, Induced Pluripotent and Adipose Stem Cells. PLoS ONE *5*, e10246.

Roode, M., Blair, K., Snell, P., Elder, K., Marchant, S., Smith, A., and Nichols, J. (2012). Human hypoblast formation is not dependent on FGF signalling. Dev. Biol. *361*, 358–363.

Schlosser, I., Hölzel, M., Hoffmann, R., Burtscher, H., Kohlhuber, F., Schuhmacher, M., Chapman, R., Weidle, U.H., and Eick, D. (2005). Dissection of transcriptional programmes in response to serum and c-Myc in a human B-cell line. Oncogene *24*, 520–524.

Selhub, J., and Miller, J.W. (1992). The pathogenesis of homocysteinemia: interruption of the coordinate regulation by S-adenosylmethionine of the remethylation and transsulfuration of homocysteine. Am. J. Clin. Nutr. *55*, 131–138.

Smith, K.N., Singh, A.M., and Dalton, S. (2010). Myc Represses Primitive Endoderm Differentiation in Pluripotent Stem Cells. Cell Stem Cell *7*, 343–354.

Sperber, H., Mathieu, J., Wang, Y., Ferreccio, A., Hesson, J., Xu, Z., Fischer, K.A., Devi, A., Detraux, D., Gu, H., et al. (2015). The metabolome regulates the epigenetic landscape during naive-to-primed human embryonic stem cell transition. Nat. Cell Biol. *17*, 1523–1535.

Subramanian, A., Tamayo, P., Mootha, V.K., Mukherjee, S., Ebert, B.L., Gillette, M.A., Paulovich, A., Pomeroy, S.L., Golub, T.R., Lander, E.S., et al. (2005). Gene set enrichment analysis: A knowledge-based approach for interpreting genome-wide expression profiles. Proc. Natl. Acad. Sci. *102*, 15545–15550.

Takahashi, K., and Yamanaka, S. (2006). Induction of Pluripotent Stem Cells from Mouse Embryonic and Adult Fibroblast Cultures by Defined Factors. Cell *126*, 663–676.

Takashima, Y., Guo, G., Loos, R., Nichols, J., Ficz, G., Krueger, F., Oxley, D., Santos, F., Clarke, J., Mansfield, W., et al. (2014). Resetting Transcription Factor Control Circuitry toward Ground-State Pluripotency in Human. Cell *158*, 1254–1269.

Thai, M., Graham, N.A., Braas, D., Nehil, M., Komisopoulou, E., Kurdistani, S.K., McCormick, F., Graeber, T.G., and Christofk, H.R. (2014). Adenovirus E4ORF1-Induced MYC Activation Promotes Host Cell Anabolic Glucose Metabolism and Virus Replication. Cell Metab. *19*, 694–701.

Theunissen, T.W., Powell, B.E., Wang, H., Mitalipova, M., Faddah, D.A., Reddy, J., Fan, Z.P., Maetzel, D., Ganz, K., Shi, L., et al. (2014). Systematic Identification of Culture Conditions for Induction and Maintenance of Naive Human Pluripotency. Cell Stem Cell *15*, 471–487.

Thomson, J.A., Itskovitz-Eldor, J., Shapiro, S.S., Waknitz, M.A., Swiergiel, J.J., Marshall, V.S., and Jones, J.M. (1998). Embryonic Stem Cell Lines Derived from Human Blastocysts. Science *282*, 1145–1147.

Thornburg, J.M., Nelson, K.K., Clem, B.F., Lane, A.N., Arumugam, S., Simmons, A., Eaton, J.W., Telang, S., and Chesney, J. (2008). Targeting aspartate aminotransferase in breast cancer. Breast Cancer Res. BCR *10*, R84.

Tohyama, S., Hattori, F., Sano, M., Hishiki, T., Nagahata, Y., Matsuura, T., Hashimoto, H., Suzuki, T., Yamashita, H., Satoh, Y., et al. (2013). Distinct Metabolic Flow Enables Large-Scale Purification of Mouse and Human Pluripotent Stem Cell-Derived Cardiomyocytes. Cell Stem Cell *12*, 127–137.

Trapnell, C., Pachter, L., and Salzberg, S.L. (2009). TopHat: discovering splice junctions with RNA-Seq. Bioinformatics *25*, 1105–1111.

Valamehr, B., Robinson, M., Abujarour, R., Rezner, B., Vranceanu, F., Le, T., Medcalf, A., Lee, T.T., Fitch, M., Robbins, D., et al. (2014). Platform for Induction and Maintenance of Transgene-free hiPSCs Resembling Ground State Pluripotent Stem Cells. Stem Cell Rep. *2*, 366–381.

Varum, S., Rodrigues, A.S., Moura, M.B., Momcilovic, O., Easley, C.A., IV, Ramalho-Santos, J., Van Houten, B., and Schatten, G. (2011). Energy Metabolism in Human Pluripotent Stem Cells and Their Differentiated Counterparts. PLoS ONE *6*, e20914.

Vassena, R., Boué, S., González-Roca, E., Aran, B., Auer, H., Veiga, A., and Belmonte, J.C.I. (2011). Waves of early transcriptional activation and pluripotency program initiation during human preimplantation development. Development *138*, 3699–3709.

Wang, X., Levi, A.J., and Halestrap, A.P. (1994). Kinetics of the sarcolemmal lactate carrier in single heart cells using BCECF to measure pHi. Am. J. Physiol. *267*, H1759–H1769.

Ware, C.B., Nelson, A.M., Mecham, B., Hesson, J., Zhou, W., Jonlin, E.C., Jimenez-Caliani, A.J., Deng, X., Cavanaugh, C., Cook, S., et al. (2014). Derivation of naïve human embryonic stem cells. Proc. Natl. Acad. Sci. *111*, 4484–4489.

Xia, X., Zhang, Y., Zieth, C.R., and Zhang, S.-C. (2007). Transgenes delivered by lentiviral vector are suppressed in human embryonic stem cells in a promoter-dependent manner. Stem Cells Dev. *16*, 167–176.

Xie, L., Tsaprailis, G., and Chen, Q.M. (2005). Proteomic identification of insulin-like growth factor-binding protein-6 induced by sublethal H2O2 stress from human diploid fibroblasts. Mol. Cell. Proteomics MCP *4*, 1273–1283.

Xiong, C., Tang, D.-Q., Xie, C.-Q., Zhang, L., Xu, K.-F., Thompson, W.E., Chou, W., Gibbons, G.H., Chang, L.-J., Yang, L.-J., et al. (2005). Genetic Engineering of Human Embryonic Stem Cells with Lentiviral Vectors. Stem Cells Dev. *14*, 367–377.

Yan, L., Yang, M., Guo, H., Yang, L., Wu, J., Li, R., Liu, P., Lian, Y., Zheng, X., Yan, J., et al. (2013). Single-cell RNA-Seq profiling of human preimplantation embryos and embryonic stem cells. Nat. Struct. Mol. Biol. *20*, 1131–1139.

Yao, S., Sukonnik, T., Kean, T., Bharadwaj, R.R., Pasceri, P., and Ellis, J. (2004). Retrovirus Silencing, Variegation, Extinction, and Memory Are Controlled by a Dynamic Interplay of Multiple Epigenetic Modifications. Mol. Ther. *10*, 27–36.

Yoshida, Y., Takahashi, K., Okita, K., Ichisaka, T., and Yamanaka, S. (2009). Hypoxia Enhances the Generation of Induced Pluripotent Stem Cells. Cell Stem Cell *5*, 237–241.

Yuan, J., Bennett, B.D., and Rabinowitz, J.D. (2008). Kinetic flux profiling for quantitation of cellular metabolic fluxes. Nat. Protoc. *3*, 1328–1340.

Zeller, K.I., Jegga, A.G., Aronow, B.J., O'Donnell, K.A., and Dang, C.V. (2003). An integrated database of genes responsive to the Myc oncogenic transcription factor: identification of direct genomic targets. Genome Biol. *4*, R69.

Zhang, J., Khvorostov, I., Hong, J.S., Oktay, Y., Vergnes, L., Nuebel, E., Wahjudi, P.N., Setoguchi, K., Wang, G., Do, A., et al. (2011). UCP2 regulates energy metabolism and differentiation potential of human pluripotent stem cells. EMBO J. *30*, 4860–4873.

Zhang, J., Nuebel, E., Daley, G.Q., Koehler, C.M., and Teitell, M.A. (2012). Metabolic Regulation in Pluripotent Stem Cells during Reprogramming and Self-Renewal. Cell Stem Cell *11*, 589–595.

Zhao, B., Ye, X., Yu, J., Li, L., Li, W., Li, S., Yu, J., Lin, J.D., Wang, C.-Y., Chinnaiyan, A.M., et al. (2008). TEAD mediates YAP-dependent gene induction and growth control. Genes Dev. *22*, 1962–1971.

Zhou, W., Choi, M., Margineantu, D., Margaretha, L., Hesson, J., Cavanaugh, C., Blau, C.A., Horwitz, M.S., Hockenbery, D., Ware, C., et al. (2012). HIF1α induced switch from bivalent to exclusively glycolytic metabolism during ESC-to-EpiSC/hESC transition. EMBO J. *31*, 2103–2116.

Zwaka, T.P., and Thomson, J.A. (2003). Homologous recombination in human embryonic stem cells. Nat. Biotechnol. *21*, 319–321.